RSC Advances

PAPER

View Article Online
View Journal | View Issue

Cite this: *RSC Adv.*, 2025, **15**, 4636

Synthesis and application of a bimetallic-MOFs with sulfonic acid tags in preparation of biologically active nicotinonitriles *via* cooperative vinylogous anomeric-based oxidation†

Milad Mohammadi Rasooll,[a] Hossein Ahmadi,[a] Hassan Sepehrmansourie,*[b] Mohammad Ali Zolfigol,*[a] Elaheh Ghytasranjbar[c] and Abdolmajid Mohammadzadeh[c]

Bimetallic-organic frameworks (bimetallic-MOFs) have broad capabilities owing to the synergistic properties of two metals in a single structure. In this regard, we prepared a bimetallic-MOF containing iron (Fe) and nickel (Ni) metals. The prepared bimetallic-MOF was functionalized with sulfonic acid groups *via* a post-modification method. Thus, a new acidic catalyst with special abilities was prepared. The physicochemical properties of the bimetallic-MOF containing sulfonic acid groups were investigated through FT-IR, SEM, BET/BJH, XRD, EDS, elemental mapping and TGA/DTG analyses. According to the acidic active sites in the structure of the presented catalyst, we investigated the performance of this catalyst in the synthesis of nicotinonitrile derivatives. The structure of the products was also confirmed using melting point, FT-IR, HR-mass, ^{1}H-NMR, and ^{13}C-NMR analyses. Moreover, the antibacterial properties of the synthesized product and MIL-88B(Fe_2/Ni)/imidazole/SO_3H were investigated, and results showed satisfactory antibacterial properties of these compounds against Gram-positive and Gram-negative bacteria.

Received 21st October 2024
Accepted 18th January 2025

DOI: 10.1039/d4ra07521h

rsc.li/rsc-advances

Introduction

Metal–organic frameworks (MOFs) are porous compounds with excellent design capabilities and controllable properties and have attracted increasing interest in many research fields in recent decades.[1,2] MOFs are also called porous coordination polymers (PCPs) and are obtained by covalently connecting metal clusters to organic ligands and creating a crystalline structure.[3,4] The broad features of MOFs include high thermal stability, high porosity, crystalline nature, and adjustable pores. These properties have made them suitable platforms and ideal chemicals for use in various fields, including gas storage, targeted drug delivery, absorption, desorption, sensors, photocatalysts, and catalysts.[5–7] Meanwhile, bimetallic-organic frameworks (bimetallic-MOFs) are an emerging category of MOFs that have special and attractive properties owing to the simultaneous presence of two metals in a single MOF structure.[8,9] In addition to possessing all the characteristics and applications of MOFs based on one metal, owing to the simultaneous presence of two metals in the crystal structure of these porous compounds, they benefit from a synergistic effect between the two metals. Furthermore, their high pore volume, highly regular pores, large number of active sites, and appropriate surface area have prompted the use of bimetallic-MOFs in many adsorption and catalytic applications.[10–12] The catalytic properties of this group of compounds can be easily changed by changing the molar ratios of their constituent metals. Thus, desired bimetallic-MOFs with suitable properties can be easily prepared.[13,14] The design capabilities of this new generation of catalysts has enabled them to be used as catalysts in many organic reactions, such as pollutant degradation, Sonogashira coupling, tandem, oxidation–reduction, and multicomponent reactions.[15–19] According to the mentioned cases, the research and development of catalysts containing two metals are attractive and promising research areas.

Therefore, we aimed to design a bimetallic catalyst based on iron (Fe) and nickel (Ni) metals, which should be an efficient catalyst considering the simultaneous presence of iron and nickel metals and their synergistic effect. The post-modification method for synthesizing MOFs is a very efficient method to obtain multi-functional catalysts. In this approach, the properties of MOFs can be changed by adding different functional groups, such as acids, amino acids, or metals.[20–25] Many

[a]*Department of Organic Chemistry, Faculty of Chemistry and Petroleum Sciences, Bu-Ali Sina University, Hamedan 6517838683, Iran. E-mail: zolfi@basu.ac.ir; mzolfigol@yahoo.com; Fax: +988138380709; Tel: +988138282807*

[b]*Faculty of Converging Science and Technologies, University of Qom, Qom, 37185-359, Iran. E-mail: sepehr9129@yahoo.com*

[c]*Department of Pathobiology, Faculty of Veterinary Science, Bu-Ali Sina University, Hamedan, Iran*

† Electronic supplementary information (ESI) available. See DOI: https://doi.org/10.1039/d4ra07521h

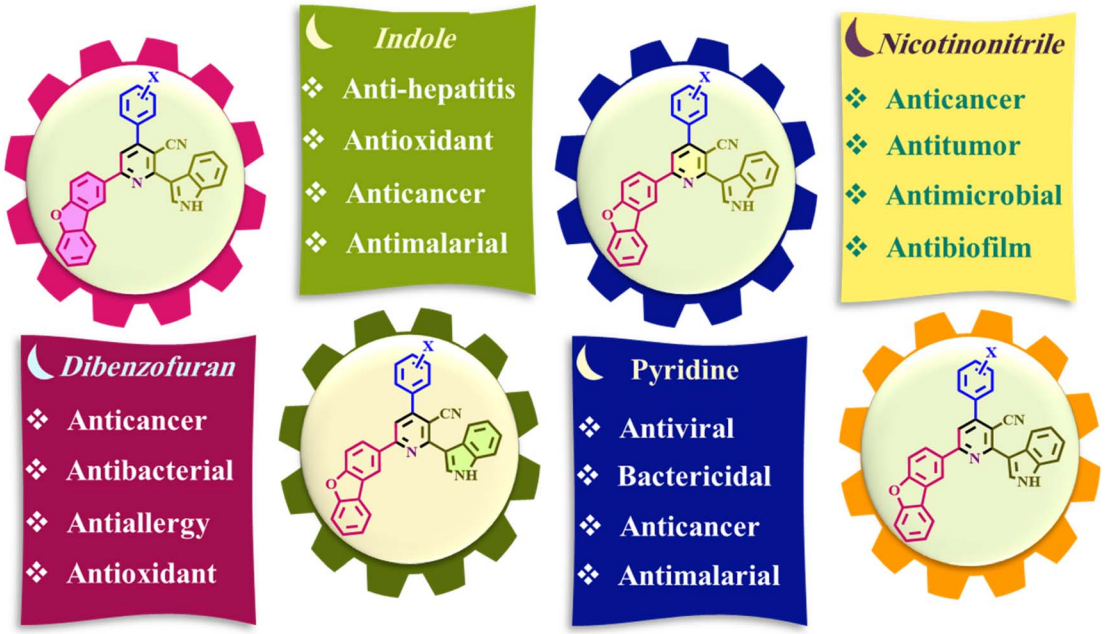

Fig. 1 Various properties of dibenzofuran, indole, pyridine and nicotinonitrile compounds.

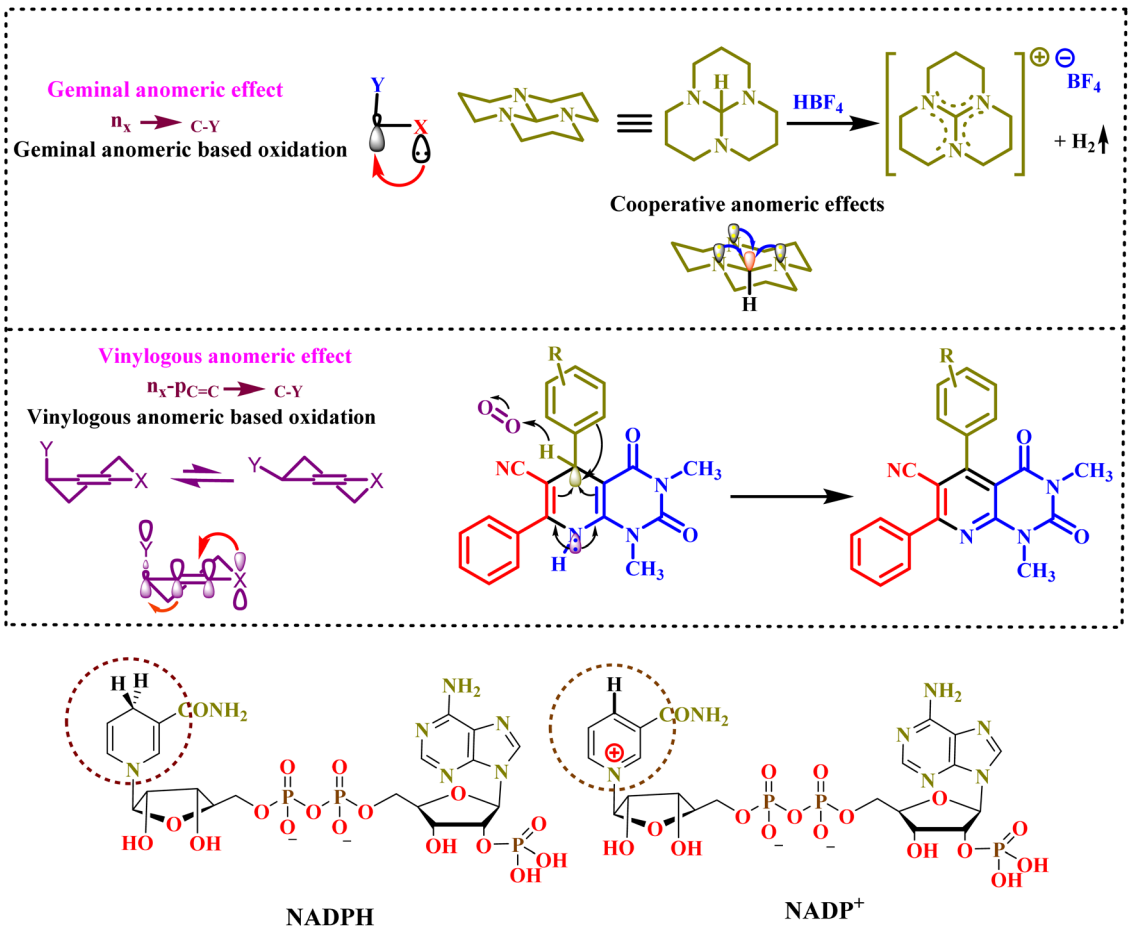

Fig. 2 Geminal *versus* vinylogous anomeric effect in the course of organic synthesis with biological activities.

heterocyclic compounds, such as pyrazolo[4,3-*e*]pyridines, spiro-oxindoles, and pyrazolo[3,4-*b*]pyridine-5-carbonitriles, have been prepared using functionalization methods. The application of MOFs is an attractive motive for the preparation of new heterocycles with mainly biological properties.[15,20,21] Therefore, we aimed to provide a rational strategy for the preparation of MIL-88B(Fe_2/Ni)/imidazole/SO_3H, which is a porous acidic catalyst, *via* a post-modification method.

In recent years, there has been increasing demand from various industrial sectors, including agriculture, paint production, and medicine, for the preparation of key compounds. Recently scientists have been paying special attention to the preparation of compounds with biological and medicinal properties. Among such compounds, nicotinitriles are of interest thanks to their biological properties, such as anticancer, antibacterial, antifungal, and antiparasitic.[26,27] On the other hand, indole, pyridine, and dibenzofuran scaffolds also have many biological and medicinal properties, such as antibacterial, antifungal, and antiparasitic, as shown in Fig. 1[28–30] The interesting biological properties of nicotinitriles gave us double motivation to prepare these compounds with the help of MIL-88B(Fe_2/Ni)/imidazole/SO_3H, which is a porous acid catalyst. Obtaining compounds with biological properties has become a very important issue in recent years. Hence, in this report, the catalytic application of MIL-88B(Fe_2/Ni)/imidazole/SO_3H as a bimetallic catalyst was investigated for the synthesis of nicotinitriles under green, mild, solvent-free conditions. It should be noted that the synthesis of the above compounds was facilitated based on the anomeric-based oxidation mechanism.

Recently, the concept of the "anomeric effect" (AE) as a stereoelectronic effect has attracted a lot of attention.[31,32] This effect can be clearly seen in heterocycles containing nitrogen (N) and oxygen (O) atoms. The mechanisms of many organic reactions have been reported based on this effect. One of the famous categories of AE is the cooperative anomeric effect, which describes the electron transfer of a lone pair from more than one heteroatom to one antibonding orbital of an acceptor atom. In another approach, the anomeric effect was applied through a double bond, which is called the vinylogous anomeric effect.[33,34] On the other hand, in the case of the vinylogous anomeric effect, a double bond acts as a bridge between the donor and acceptor orbitals. Recently, the concept of "cooperative vinylogous anomeric-based oxidation" (CVABO) was put forward based on the above two terms, which includes a new tactic for the oxidation of organic compounds in the absence of any oxidizing agents.[35,36] The oxidation of compounds in the course of reaction *via* the anomeric support has been named anomeric-based oxidation (ABO).[33,34] It is worth mentioning that the oxidation/reduction of many biological systems, such as $NADP^+$/NADPH or NAD^+/NADH, proceeds through CVABO (Fig. 2).[37]

Experimental section

Materials and methods

$Ni(NO_3)_2\cdot 6H_2O$ (Sigma-Aldrich), $FeCl_3\cdot 6H_2O$ (Sigma-Aldrich, 99%), terephthalic acid (H_2-BDC, 98%), sodium hydroxide (Merck), imidazole ($C_3N_2H_4$, 99%), chlorosulfuric acid (Sigma-Aldrich, 99%), dibenzofuran ($C_{12}H_8O$, 95%), acetyl chloride (Sigma-Aldrich, 98%), aluminum chloride ($AlCl_3$, 99%), indole (C_8H_7N, 99%), acetic anhydride ($C_4H_6O_3$, 95%), cyano acetic acid ($C_3H_3NO_2$, 99%), ammonium acetate (Sigma-Aldrich, 97%), and various aromatic aldehyde derivatives (95%) were purchased from Merck and Sigma-Aldrich. Furthermore, *N*,*N*-dimethylformamide (DMF, 99%), ethanol (EtOH, 99%), methanol (MeOH, 99%), acetonitrile (CH_3CN, 99%), dichloromethane (CH_2Cl_2, 99%), and other solvents were purchased from commercial sources without further purification. The required precursors were synthesized according to our recently reported educational synthetic organic theory.[38]

Characterization

The X-ray powder diffraction (XRD) technique was applied on a PHILIPS PW1730 instrument (Netherlands) to characterize the crystal planes of the catalyst. High-resolution mass spectroscopy was performed using a Waters Micromass, LCT Premier mass spectrometer, USA. FT-IR (PerkinElmer Spectrum Version 10.02.00) was used to identify the functional groups in the different stages of the catalyst. Moreover, the morphology of the different stages of the catalyst was characterized by scanning electron microscopy (SEM) as well as energy-dispersive spectroscopy (EDS), while elemental mapping was carried out using a Zeiss Sigma VP system (Germany). In addition, the thermal and chemical stability of the synthesized catalyst were determined by thermogravimetry/differential thermogravimetric analysis (TGA/DTG) technique (TGA2 Mettler Toledo). Finally, Brunauer–Emmett–Teller (BET, BELSORP-mini-II) method was applied using the British Journal of Haematology (BJH) technique on a BELSORP-mini-II analyzer to determine the surface areas and pore sizes of the synthesized catalysts.

Preparation of MIL-88B(Fe_2/Ni)

In order to research and develop bimetallic-MOFs as a new generation of MOFs, we prepared MIL-88B(Fe_2/Ni) based on a previous report.[39] To achieve this goal, first $Ni(NO_3)_2\cdot 6H_2O$ (0.33 mmol, 0.096 g) and $FeCl_3\cdot 6H_2O$ (1.33 mmol, 0.359 g) were dissolved in DMF (5 mL) and solution (A) was obtained. Then, in another round-bottom flask, terephthalic acid (2 mmol, 0.33 g) was dissolved in DMF (5 mL) to give solution (B). Next, solution A along with 0.4 mol L^{-1} NaOH solution (2 mL) was added to solution B and the resulting mixture was stirred for 15 min at room temperature. Finally, the resulting solution was transferred into a Teflon-lined autoclave (60 mL) and placed in an oven at 100 °C for 20 h. After centrifugation followed by washing several times with DMF, MeOH/DMF (1 : 1), and MeOH, the resulting precipitate was dried at 80 °C.

Preparation of MIL-88B(Fe_2/Ni)/imidazole/SO_3H as a new porous catalyst

After the preparation and purification of MIL-88B(Fe_2/Ni), the catalyst needed to be activated. To do this, the as-obtained precipitate was placed in a vacuum oven at 150 °C for 24 h. Then, in a 50 mL round-bottom flask, a mixture of MIL-88B(Fe_2/Ni) (1 g), imidazole (10 mmol, 0.68 g), and acetonitrile (CH_3CN,

20 mL) was refluxed for 12 h. After centrifugation followed washing several times with acetonitrile, the precipitate was filtered off and dried. Then, 0.5 g of MIL-88B(Fe_2/Ni)/imidazole obtained in the previous step was dispersed in CH_2Cl_2 at 0 °C. Finally, chlorosulfonic acid (2 mmol, 0.133 mL) was added dropwise to the above mixture and the contents of the flask were stirred for 30 min (at room temperature). After washing with CH_2Cl_2 and EtOH several times, MIL-88B(Fe_2/Ni)/imidazole/SO_3H was obtained by centrifugation and then dried at room temperature (Scheme 1).

Catalytic reaction

After the synthesis of MIL-88B(Fe_2/Ni)/imidazole/SO_3H, which is a new acid catalyst, the catalytic application of the above bimetallic-MOF was investigated in the preparation of nicotinonitrile compounds. For this purpose, initially 3-(1*H*-indol-3-yl)-3-oxopropanenitrile and 1-(dibenzo[*b*,*d*]furan-2-yl)ethan-1-one were synthesized as starting materials according to previous reports.[40,41] Then, 3-(1*H*-indol-3-yl)-3-oxopropanenitrile (1 mmol, 0.184 g), 1-(dibenzo[*b*,*d*]furan-2-yl) ethan-1-one (1 mmol, 0.21 g), ammonium acetate (1.5 mmol, 0.11 g), and an aldehyde (1 mmol) along with 20 mg of MIL-88B(Fe_2/Ni)/imidazole/SO_3H as a catalyst were placed in a round-bottomed flask under solvent-free conditions and heated at 100 °C. The progress of the reaction was followed by TLC (*n*-hexane/ethyl acetate). After the completion of the reaction, hot EtOH was added to the reaction mixture in aid separation of the catalyst from the reaction product. Next, the catalyst was separated from the reaction mixture using a centrifuge. Finally, after the evaporation of the solvent, the precipitate was washed several times with EtOH and purified (Scheme 2).

Antibacterial activity

The antibacterial activity of the MIL-88B(Fe_2/Ni)/imidazole/SO_3H and compound A1 were evaluated. The compounds were tested on *Escherichia coli* (ATCC 25922), *Staphylococcus aureus* (ATCC 5923), and an isolated methicillin-resistant *Staphylococcus aureus* (MRSA), representing both Gram-positive and -negative bacteria, and evaluated by the colony forming unit (CFU) method (details of the presented method are available in the ESI†).

Spectral data of the nicotinonitrile derivatives

6-(Dibenzo[*b*,*d*]furan-2-yl)-4-(3,4-dimethoxyphenyl)-2-(1*H*-indol-3-yl)nicotinonitrile (A1). Yellow solid; Mp: 296–298 °C; FT-IR (KBr, cm^{-1}): 3337, 2213, 1609, 1569, 1526. ^{1}H NMR (400 MHz, DMSO-d_6) δ_{ppm} 11.87 (d, 1H), 9.14 (d, J = 1.5 Hz, 1H), 8.59 (dd, J = 8.7, 1.7 Hz, 1H), 8.47 (dd, J = 6.4, 2.7 Hz, 1H), 8.42 (d, J = 2.9 Hz, 1H), 8.24 (d, J = 7.5 Hz, 1H), 8.13 (s, 1H), 7.92 (d, J = 8.7 Hz, 1H), 7.77 (d, J = 8.2 Hz, 1H), 7.61–7.57 (m, 2H), 7.50–7.47 (m, 2H), 7.45 (d, J = 2.2 Hz, 1H), 7.30–7.27 (m, 2H), 7.20 (d, J = 8.4 Hz, 1H), 3.92 (s, 3H), 3.89 (s, 3H). ^{13}C NMR (101 MHz, DMSO-d_6) δ_{ppm} 157.9, 157.4, 156.8, 156.1, 154.9, 150.1, 148.6, 136.3, 133.0, 129.1, 128.7, 128.1, 127.2, 126.1, 124.3, 123.5, 123.4, 122.3, 121.8, 121.4, 121.3, 120.8, 120.6, 119.3, 116.2, 113.1, 112.7, 112.2, 112.1, 111.9, 111.7, 101.1, 55.8, 55.7. HRMS (ESI†) m/z $[M + H]^+$ calcd for $[C_{34}H_{23}N_3O_3 + H]^+$, 522.1812; found, 522.1743.

6-(Dibenzo[*b*,*d*]furan-2-yl)-2-(1*H*-indol-3-yl)-4-(4-methoxyphenyl)nicotinonitrile (A2). Yellow solid; Mp: 290–292 °C; FT-IR (KBr, cm^{-1}): 3259, 2190, 1615, 1537, 1509. ^{1}H NMR (400 MHz, DMSO-d_6) δ_{ppm} 11.86 (s, 1H), 9.13 (s, 1H), 8.58 (dd, 1H), 8.47–8.44 (m, 1H), 8.40 (d, J = 2.7 Hz, 1H), 8.24 (d, J = 7.5 Hz, 1H), 8.08 (s, 1H), 7.91 (d, J = 8.7 Hz, 1H), 7.83 (d, J = 8.6 Hz, 2H), 7.76 (d, J = 8.2 Hz, 1H), 7.58 (t, J = 7.2 Hz, 2H), 7.47 (t, J = 7.5 Hz, 1H), 7.30–7.26 (m, 2H), 7.19 (d, J = 8.7 Hz, 2H), 3.89 (s, 3H). ^{13}C NMR (101 MHz, DMSO-d_6) δ_{ppm} 160.5, 157.9, 157.4, 156.8, 156.1, 154.7, 136.4, 133.0, 130.5, 129.0, 128.6, 128.0, 127.2, 126.1, 124.3, 123.5, 122.3, 121.3, 121.3, 120.7, 120.5, 119.2, 116.2, 114.16, 113.1, 112.1, 112.1, 111.9, 101.0, 55.4. HRMS (ESI†) m/z $[M + H]^+$ calcd for $[C_{33}H_{21}N_3O_2 + H]^+$, 492.1707; found, 492.1612.

4-(4-Chlorophenyl)-6-(dibenzo[*b*,*d*]furan-2-yl)-2-(1*H*-indol-3-yl)nicotinonitrile (A3). Yellow solid; Mp: >300 °C; FT-IR (KBr, cm^{-1}): 3293, 2220, 1591, 1512, 1485. ^{1}H NMR (400 MHz, DMSO-d_6) δ_{ppm} 11.88 (d, J = 3.0 Hz, 1H), 9.13 (d, J = 1.9 Hz, 1H), 8.58 (dd, J = 8.7, 2.0 Hz, 1H), 8.48–8.45 (m, 1H), 8.40 (d, J = 3.0 Hz, 1H), 8.22 (d, J = 7.2 Hz, 1H), 8.12 (s, 1H), 7.92–7.88 (m, 2H), 7.87 (s, 1H), 7.76 (d, J = 8.2 Hz, 1H), 7.71 (d, J = 8.6 Hz, 2H), 7.60–7.56 (m, 2H), 7.47 (t, J = 7.2 Hz, 1H), 7.31–7.27 (m, 2H). ^{13}C NMR (101 MHz, DMSO-d_6) δ_{ppm} 158.1, 157.3, 156.8, 156.1, 153.8, 136.4, 135.7, 134.7, 132.8, 130.9, 130.9, 128.7, 128.1, 127.2, 126.0, 124.3, 123.5, 123.4, 122.4, 121.3, 120.8, 120.6, 118.8, 116.3, 113.0, 112.2, 112.1, 111.9, 101.1.

6-(Dibenzo[*b*,*d*]furan-2-yl)-4-(4-hydroxy-3-methoxyphenyl)-2-(1*H*-indol-3-yl)nicotinonitrile (A4). Yellow solid; Mp: 280–282 °C; FT-IR (KBr, cm^{-1}): 3446, 3170, 2188, 1614, 1536. ^{1}H NMR (400 MHz, DMSO-d_6) δ_{ppm} 11.87 (d, 1H), 9.65 (s, 1H), 9.15 (d, J = 1.4 Hz, 1H), 8.59 (dd, J = 8.7, 1.7 Hz, 1H), 8.46 (dd, J = 6.4, 2.6 Hz, 1H), 8.41 (d, J = 2.8 Hz, 1H), 8.25 (d, J = 7.5 Hz, 1H), 8.12 (s, 1H), 7.92 (d, J = 8.7 Hz, 1H), 7.77 (d, J = 8.2 Hz, 1H), 7.61–7.56 (m, 2H), 7.50–7.46 (m, 2H), 7.33 (dd, J = 8.1, 2.0 Hz, 1H), 7.30–7.26 (m, 2H), 7.03 (d, J = 8.2 Hz, 1H), 3.94 (s, 3H). ^{13}C NMR (101 MHz, DMSO-d_6) δ_{ppm} 157.8, 157.5, 156.7, 156.1, 155.1, 148.3, 147.6, 136.3, 133.1, 128.7, 128.0, 127.7, 127.2, 126.1, 124.3, 123.5, 123.5, 122.3, 122.1, 121.4, 121.3, 120.7, 120.5, 119.4, 116.2, 115.6, 113.3, 113.1, 112.1, 112.1, 111.9, 101.1, 55.9. HRMS (ESI†) m/z $[M + H]^+$ calcd for $[C_{33}H_{21}N_3O_3 + H]^+$, 508.1656; found, 508.1594.

6-(Dibenzo[*b*,*d*]furan-2-yl)-2-(1*H*-indol-3-yl)-4-phenylnicotinonitrile (A5). Yellow solid; Mp: 260–262 °C; FT-IR (KBr, cm^{-1}): 3347, 2217, 1569, 1529, 1479. ^{1}H NMR (400 MHz, DMSO-d_6) δ_{ppm} 11.89 (s, 1H), 9.18 (d, J = 1.5 Hz, 1H), 8.62 (dd, J = 8.7, 1.8 Hz, 1H), 8.46 (dd, J = 6.4, 2.7 Hz, 1H), 8.41 (d, J = 2.9 Hz, 1H), 8.26 (d, J = 7.3 Hz, 1H), 8.16 (s, 1H), 7.94 (d, J = 8.7 Hz, 1H), 7.89–7.86 (m, 2H), 7.79 (d, J = 8.2 Hz, 1H), 7.69–7.64 (m, 3H), 7.61–7.56 (m, 2H), 7.48 (t, J = 7.5 Hz, 1H), 7.31–7.27 (m, 2H). ^{13}C NMR (101 MHz, DMSO-d_6) δ_{ppm} 158.1, 157.4, 156.8, 156.1, 155.1, 137.0, 136.4, 132.9, 129.7, 129.0, 128.7, 128.7, 128.1, 127.2, 126.1, 124.3, 123.5, 123.5, 122.4, 121.4, 121.3, 120.8, 120.7, 118.9, 116.4, 113.0, 112.2, 112.1, 111.9, 101.2.

HRMS (ESI†) *m/z* $[M + H]^+$ calcd for $[C_{32}H_{19}N_3O + H]^+$, 462.1601; found, 462.1536.

6-(Dibenzo[*b*,*d*]furan-2-yl)-2-(1*H*-indol-3-yl)-[4,4′-bipyridine]-3-carbonitrile (A6). Yellow solid; Mp: 296–298 °C; FT-IR (KBr, cm^{-1}): 3394, 2184, 1654, 1514, 1458. ^{1}H NMR (400 MHz, DMSO-d_6) δ_{ppm} 11.92 (d, 1H), 9.18 (d, J = 1.5 Hz, 1H), 8.87 (dd, J = 4.6, 1.3 Hz, 2H), 8.62 (dd, J = 8.7, 1.8 Hz, 1H), 8.48–8.46 (m, 1H), 8.42 (d, J = 2.9 Hz, 1H), 8.25–8.21 (m, 2H), 7.95 (d, J = 8.7 Hz, 1H), 7.88 (dd, J = 4.5, 1.5 Hz, 2H), 7.79 (d, J = 8.2 Hz, 1H), 7.62–7.58 (m, 2H), 7.49 (t, J = 7.3 Hz, 1H), 7.31–7.28 (m, 2H). ^{13}C NMR (101 MHz, DMSO-d_6) δ_{ppm} 158.4, 157.3, 156.9, 156.1, 152.5, 150.1, 144.4, 136.4, 132.6, 128.9, 128.2, 127.3, 126.0, 124.3, 123.6, 123.5, 123.4, 122.5, 121.3, 121.3, 120.9, 120.7, 118.4, 116.1, 112.9, 112.3, 112.2, 111.9, 100.7. HRMS (ESI†) *m/z* $[M + H]^+$ calcd for $[C_{31}H_{18}N_4O + H]^+$, 463.1553; found, 463.1466.

6-(Dibenzo[*b*,*d*]furan-2-yl)-2-(1*H*-indol-3-yl)-4-(naphthalen-2-yl)nicotinonitrile (A7). Yellow solid; Mp: >300 °C; FT-IR (KBr, cm^{-1}): 3444, 2216, 1599, 1566, 1532. ^{1}H NMR (400 MHz, DMSO-d_6) δ_{ppm} 11.92 (s, 1H), 9.18 (s, 1H), 8.62 (d, J = 8.1 Hz, 1H), 8.51 (s, 1H), 8.44 (d, J = 12.1 Hz, 2H), 8.26–8.16 (m, 3H), 8.10 (s, 2H), 7.95 (dd, J = 17.5, 8.2 Hz, 2H), 7.77 (d, J = 7.4 Hz, 1H), 7.68 (s, 2H), 7.60 (s, 2H), 7.46 (s, 1H), 7.30 (s, 2H). ^{13}C NMR (101 MHz, DMSO-d_6) δ_{ppm} 158.1, 157.4, 156.8, 156.1, 155.1, 136.4, 134.4, 133.1, 132.9, 132.6, 128.7, 128.6, 128.5, 128.3, 128.1, 127.7, 127.4, 127.2, 126.9, 126.3, 126.1, 124.3, 123.5, 123.4, 122.4, 121.4, 120.8, 120.6, 119.0, 116.6, 113.1, 112.2, 112.2, 111.9, 101.3. HRMS (ESI†) *m/z* $[M + H]^+$ calcd for $[C_{36}H_{21}N_3O + H]^+$, 512.1757; found, 512.1684.

6-(Dibenzo[*b*,*d*]furan-2-yl)-2-(1*H*-indol-3-yl)-4-(*o*-tolyl)nicotinonitrile (A8). Yellow solid; Mp: 280–282 °C; FT-IR (KBr, cm^{-1}): 3420, 2194, 1613, 1591, 1460. ^{1}H NMR (400 MHz, DMSO-d_6) δ_{ppm} 11.90 (s, 1H), 9.18 (s, 1H), 8.63 (d, J = 9.8 Hz, 1H), 8.52 (dd, J = 6.0, 2.8 Hz, 1H), 8.41 (d, J = 2.8 Hz, 1H), 8.24 (d, J = 7.6 Hz, 1H), 8.09 (s, 1H), 7.93 (d, J = 8.7 Hz, 1H), 7.77 (d, J = 8.2 Hz, 1H), 7.58 (t, J = 7.9 Hz, 2H), 7.50–7.45 (m, 4H), 7.43 (dd, J = 7.9, 3.1 Hz, 1H), 7.32–7.28 (m, 2H), 2.33 (s, 3H). ^{13}C NMR (101 MHz, DMSO-d_6) δ_{ppm} 157.9, 156.8, 156.8, 156.1, 155.7, 137.1, 136.4, 135.1, 132.8, 130.4, 129.2, 129.0, 128.6, 128.1, 127.2, 126.1, 126.0, 124.3, 123.5, 123.5, 122.4, 121.4, 120.9, 120.7, 118.3, 116.6, 112.9, 112.2, 112.2, 111.9, 102.3, 19.6. HRMS (ESI†) *m/z* $[M + H]^+$ calcd for $[C_{33}H_{21}N_3O + H]^+$, 476.1757; found, 476.1703.

4-(4-Bromophenyl)-6-(dibenzo[*b*,*d*]furan-2-yl)-2-(1*H*-indol-3-yl)nicotinonitrile (A9). Yellow solid; Mp: >300 °C; FT-IR (KBr, cm^{-1}): 3342, 2215, 1590, 1526, 1437. ^{1}H NMR (400 MHz, DMSO-d_6) δ_{ppm} 11.89 (d, 1H), 9.13 (d, J = 1.5 Hz, 1H), 8.57 (dd, J = 8.7, 1.8 Hz, 1H), 8.47–8.44 (m, 1H), 8.40 (d, J = 2.9 Hz, 1H), 8.22 (d, J = 7.5 Hz, 1H), 8.12 (s, 1H), 7.91 (d, J = 8.7 Hz, 1H), 7.84–7.81 (m, 3H), 7.80–7.74 (m, 2H), 7.61–7.57 (m, 2H), 7.47 (t, J = 7.5 Hz, 1H), 7.30–7.27 (m, 2H). ^{13}C NMR (101 MHz, DMSO-d_6) δ_{ppm} 158.1, 157.3, 156.8, 156.1, 153.9, 153.8, 136.4, 136.1, 132.7, 131.7, 131.2, 131.1, 128.8, 128.1, 127.2, 126.0, 124.3, 123.5, 123.4, 123.4, 122.4, 121.3, 120.8, 120.6, 118.8, 116.2, 113.0, 112.2, 112.1, 111.9, 101.0. HRMS (ESI†) *m/z* $[M + H]^+$ calcd for $[C_{32}H_{18}BrN_3O + H]^+$, 540.0706; found, 540.0671.

6-(Dibenzo[*b*,*d*]furan-2-yl)-4-(2,4-dichlorophenyl)-2-(1*H*-indol-3-yl)nicotinonitrile (A10). Yellow solid; Mp: 260–262 °C; FT-IR (KBr, cm^{-1}): 3330, 2216, 1587, 1573, 1473. ^{1}H NMR (400 MHz, DMSO-d_6) δ_{ppm} 11.94 (d, 1H), 9.15 (d, 1H), 8.60 (dd, J = 8.7, 1.5 Hz, 1H), 8.51 (dd, J = 6.1, 2.9 Hz, 1H), 8.40 (d, J = 2.8 Hz, 1H), 8.22 (d, J = 7.6 Hz, 1H), 8.16 (s, 1H), 8.06–7.88 (m, 2H), 7.77 (d, J = 8.4 Hz, 2H), 7.71 (dd, J = 8.3, 1.9 Hz, 1H), 7.62–7.57 (m, 2H), 7.48 (t, J = 7.5 Hz, 1H), 7.32–7.28 (m, 2H). ^{13}C NMR (101 MHz, DMSO-d_6) δ_{ppm} 158.3, 156.9, 156.7, 156.1, 152.1, 136.4, 135.1, 135.0, 132.8, 132.5, 132.4, 129.3, 128.6, 128.1, 127.9, 127.1, 125.9, 124.4, 123.6, 123.4, 122.5, 121.3, 121.0, 120.7, 117.9, 116.7, 112.8, 112.3, 112.2, 111.9, 102.2. HRMS (ESI†) *m/z* $[M + H]^+$ calcd for $[C_{32}H_{17}Cl_2N_3O + H]^+$, 530.0821; found, 530.0789.

4-(4-Cyanophenyl)-6-(dibenzo[*b*,*d*]furan-2-yl)-2-(1*H*-indol-3-yl)nicotinonitrile (A11). Yellow solid; Mp: >300 °C; FT-IR (KBr, cm^{-1}): 3332, 2224, 2215, 1573, 1439. ^{1}H NMR (250 MHz, DMSO-d_6) δ_{ppm} 11.88 (s, 1H), 9.12 (s, 1H), 8.57 (d, J = 7.6 Hz, 1H), 8.40 (d, J = 10.8 Hz, 2H), 8.19 (d, J = 7.5 Hz, 1H), 8.12 (d, J = 11.6 Hz, 3H), 8.04 (d, J = 6.9 Hz, 2H), 7.90 (d, J = 7.9 Hz, 1H), 7.75 (d, J = 7.4 Hz, 1H), 7.56 (s, 2H), 7.45 (t, 1H), 7.25 (s, 2H). ^{13}C NMR (63 MHz, DMSO-d_6) δ_{ppm} 158.5, 157.5, 156.3, 153.8, 141.9, 136.8, 133.1, 130.5, 129.3, 128.6, 127.7, 126.4, 124.4, 124.0, 122.9, 121.7, 121.4, 121.1, 119.0, 116.7, 113.2, 112.7, 112.4, 101.4. HRMS (ESI†) *m/z* $[M + H]^+$ calcd for $[C_{33}H_{18}N_4O + H]^+$, 487.1553; found, 487.1483.

6-(Dibenzo[*b*,*d*]furan-2-yl)-4-(3-hydroxyphenyl)-2-(1*H*-indol-3-yl)nicotinonitrile (A12). Yellow solid; Mp: 278–280 °C; FT-IR (KBr, cm^{-1}): 3500, 3426, 2218, 1595, 1423. ^{1}H NMR (400 MHz, DMSO-d_6) δ_{ppm} 11.88 (d, 1H), 9.90 (s, 1H), 9.15 (d, 1H), 8.59 (dd, J = 8.7, 1.6 Hz, 1H), 8.48–8.45 (m, 1H), 8.41 (d, J = 2.8 Hz, 1H), 8.24 (d, J = 7.6 Hz, 1H), 8.10 (s, 1H), 7.90 (d, J = 8.7 Hz, 1H), 7.76 (d, J = 8.2 Hz, 1H), 7.61–7.56 (m, 2H), 7.45 (q, J = 7.8 Hz, 2H), 7.31–7.27 (m, 2H), 7.25–7.21 (m, 2H), 7.03 (dd, 1H). ^{13}C NMR (101 MHz, DMSO-d_6) δ_{ppm} 158.0, 157.5, 157.3, 156.8, 156.1, 155.2, 138.3, 136.4, 132.8, 129.9, 128.7, 128.0, 127.2, 126.1, 124.3, 123.5, 122.4, 121.4, 121.3, 120.8, 120.6, 119.5, 118.9, 116.6, 116.2, 115.6, 113.0, 112.2, 111.8, 101.1. HRMS (ESI†) *m/z* $[M + H]^+$ calcd for $[C_{32}H_{19}N_3O_2 + H]^+$, 478.1550; found, 478.1478.

6-(Dibenzo[*b*,*d*]furan-2-yl)-2-(1*H*-indol-3-yl)-4-(3-nitrophenyl)nicotinonitrile (A13). Yellow solid; Mp: 286–288 °C; FT-IR (KBr, cm^{-1}): 3376, 2219, 1582, 1531, 1347. ^{1}H NMR (400 MHz, DMSO-d_6) δ_{ppm} 11.91 (d, 1H), 9.13 (d, 1H), 8.72 (s, 1H), 8.59 (dd, J = 8.7, 1.7 Hz, 1H), 8.49–8.45 (m, 2H), 8.42 (d, J = 2.8 Hz, 1H), 8.32 (d, J = 7.8 Hz, 1H), 8.21 (d, J = 9.3 Hz, 2H), 7.95–7.90 (m, 2H), 7.76 (d, J = 8.2 Hz, 1H), 7.60–7.56 (m, 2H), 7.47 (t, J = 7.5 Hz, 1H), 7.31–7.27 (m, 2H). ^{13}C NMR (101 MHz, DMSO-d_6) δ_{ppm} 158.3, 157.3, 156.9, 156.1, 152.6, 147.8, 138.3, 136.4, 135.7, 132.7, 130.4, 128.9, 128.1, 127.2, 126.0, 124.4, 124.3, 123.8, 123.5, 123.4, 122.4, 121.3, 120.9, 120.6, 118.6, 116.4, 112.9, 112.2, 112.2, 111.9, 101.1. HRMS (ESI†) *m/z* $[M + H]^+$ calcd for $[C_{32}H_{18}N_4O_3 + H]^+$, 507.1452; found, 507.1385.

6-(Dibenzo[*b*,*d*]furan-2-yl)-2-(1*H*-indol-3-yl)-4-(4-nitrophenyl)nicotinonitrile (A14). Yellow solid; Mp: 268–270 °C; FT-IR (KBr, cm^{-1}): 3442, 2192, 1590, 1563, 1514. ^{1}H NMR (400 MHz, DMSO-d_6) δ_{ppm} 11.92 (d, 1H), 9.17 (d, J = 1.5 Hz, 1H), 8.75 (t,

1H), 8.62 (dd, J = 8.7, 1.8 Hz, 1H), 8.50–8.47 (m, 2H), 8.44 (d, J = 2.8 Hz, 1H), 8.35 (d, J = 7.9 Hz, 1H), 8.27–8.22 (m, 2H), 7.95 (d, J = 8.5 Hz, 2H), 7.79 (d, J = 8.2 Hz, 1H), 7.61–7.58 (m, 2H), 7.49 (t, J = 7.5 Hz, 1H), 7.32–7.28 (m, 2H). ^{13}C NMR (101 MHz, DMSO-d_6) δ_{ppm} 158.3, 157.3, 156.9, 156.1, 152.7, 147.9, 138.4, 136.4, 135.8, 132.7, 130.6, 130.4, 129.2, 128.9, 128.1, 127.3, 126.0, 124.4, 123.9, 123.6, 123.4, 122.5, 121.3, 120.9, 120.7, 118.6, 116.5, 112.9, 112.3, 112.2, 111.9, 101.2. HRMS (ESI†) m/z [M + H]$^+$ calcd for [$C_{32}H_{18}N_4O_3$ + H]$^+$, 507.1452; found, 507.1387.

6-(Dibenzo[*b*,*d*]furan-2-yl)-4-(4-fluorophenyl)-2-(1*H*-indol-3-yl)nicotinonitrile (A15). Yellow solid; Mp: 288–290 °C; FT-IR (KBr, cm^{-1}): 3361, 2216, 1570, 1529, 1479. ^{1}H NMR (400 MHz, DMSO-d_6) δ_{ppm} 11.89 (d, 1H), 9.15 (d, J = 1.5 Hz, 1H), 8.59 (dd, J = 8.7, 1.8 Hz, 1H), 8.48–8.44 (m, 1H), 8.40 (d, J = 2.9 Hz, 1H), 8.23 (d, J = 7.3 Hz, 1H), 8.13 (s, 1H), 7.95–7.90 (m, 3H), 7.77 (d, J = 8.2 Hz, 1H), 7.61–7.56 (m, 2H), 7.52–7.45 (m, 3H), 7.31–7.26 (m, 2H). ^{13}C NMR (101 MHz, DMSO-d_6) δ_{ppm} 164.2, 161.8, 158.1, 157.3, 156.8, 156.1, 154.0, 136.4, 133.4, 133.3, 132.8, 131.4, 131.4, 128.7, 128.1, 127.2, 126.0, 124.3, 123.5, 122.4, 121.3, 120.8, 120.6, 118.9, 116.4, 115.8, 115.6, 113.0, 112.2, 112.1, 111.9, 101.2. HRMS (ESI†) m/z [M + H]$^+$ calcd for [$C_{32}H_{18}FN_3O$ + H]$^+$, 480.1507; found, 480.1459.

6-(Dibenzo[*b*,*d*]furan-2-yl)-2-(1*H*-indol-3-yl)-4-(*p*-tolyl)nicotinonitrile (A16). Yellow solid; Mp: 262–264 °C; FT-IR (KBr, cm^{-1}): 3333, 2216, 1589, 1572, 1478. ^{1}H NMR (400 MHz, DMSO-d_6) δ_{ppm} 11.88 (d, 1H), 9.16 (d, J = 1.5 Hz, 1H), 8.59 (dd, J = 8.7, 1.8 Hz, 1H), 8.47–8.44 (m, 1H), 8.40 (d, J = 2.9 Hz, 1H), 8.25 (d, J = 7.5 Hz, 1H), 8.12 (s, 1H), 7.93 (d, J = 8.7 Hz, 1H), 7.79–7.75 (m, 3H), 7.61–7.57 (m, 2H), 7.50–7.45 (m, 3H), 7.30–7.26 (m, 2H), 2.46 (s, 3H). ^{13}C NMR (101 MHz, DMSO-d_6) δ_{ppm} 158.0, 157.4, 156.8, 156.1, 155.1, 139.5, 136.3, 134.1, 132.9, 129.3, 128.9, 128.7, 128.1, 127.2, 126.1, 124.3, 123.5, 123.5, 122.4, 121.4, 121.3, 120.8, 120.6, 119.0, 116.3, 113.0, 112.2, 112.1, 111.9, 101.1, 20.9. HRMS (ESI†) m/z [M + H]$^+$ calcd for [$C_{33}H_{21}N_3O$ + H]$^+$, 476.1757; found, 476.1690.

6-(Dibenzo[*b*,*d*]furan-2-yl)-4-(4-hydroxyphenyl)-2-(1*H*-indol-3-yl)nicotinonitrile (A17). Yellow solid; Mp: >300 °C; FT-IR (KBr, cm^{-1}): 3404, 3303, 2219, 1610, 1569. ^{1}H NMR (400 MHz, DMSO-d_6) δ_{ppm} 11.86 (d, 1H), 10.06 (s, 1H), 9.14 (d, 1H), 8.58 (dd, J = 8.7, 1.6 Hz, 1H), 8.45–8.43 (m, 1H), 8.39 (d, J = 2.8 Hz, 1H), 8.25 (d, J = 7.5 Hz, 1H), 8.08 (s, 1H), 7.91 (d, J = 8.7 Hz, 1H), 7.78–7.72 (m, 3H), 7.60–7.56 (m, 2H), 7.48 (t, J = 7.3 Hz, 1H), 7.30–7.26 (m, 2H), 7.02 (d, J = 8.5 Hz, 2H). ^{13}C NMR (101 MHz, DMSO-d_6) δ_{ppm} 159.1, 157.9, 157.5, 156.7, 156.1, 155.0, 136.3, 133.0, 130.6, 128.6, 128.0, 127.4, 127.2, 126.1, 124.3, 123.5, 122.3, 121.4, 121.3, 120.7, 120.5, 119.3, 116.4, 116.0, 115.5, 113.1, 112.1, 112.1, 111.9, 101.2, 100.9. HRMS (ESI†) m/z [M + H]$^+$ calcd for [$C_{32}H_{19}N_3O_2$ + H]$^+$, 478.1550; found, 478.1470.

Results and discussion

In 2001, our research group introduced silica sulfuric acid (SSA) as an efficient solid alternative to liquid sulfuric acid.[42] Subsequently, SSA has been used widely as an inexpensive and eco-friendly solid acid for various purposes. It has also been cited in US patents. The catalytic applications of SSA have been comprehensively reviewed.[43] In this regard, we decided to synthesize and apply a bimetallic MOF with sulfonic acid tags MIL-88B(Fe_2/Ni)/imidazole/SO_3H for the preparation of biologically active nicotinonitrile derivatives.

Catalyst preparation strategy

In recent decades, porous catalysts have enabled new insights to be gained due to their good permeability, controlled pores, high temperature resistance, and excellent catalytic power. Therefore, our research group recently turned its attention to the study of porous catalysts.[44,45] In previous reports, the interesting features of bimetallic-MOFs, such as design ability, synergistic properties, and high catalytic power, were investigated.[15,20] Considering the, MIL-88B(Fe_2/Ni) as a porous catalyst was prepared based on iron (Fe) and nickel (Ni) metals. It should be noted that each of these metals creates interesting characteristics for the catalyst. Next, with the help of post-modification techniques, sulfonic acid groups (SO_3H) were placed on the surface of the above catalyst. The structure of MIL-88B(Fe_2/Ni)/imidazole/SO_3H as a new acid catalyst was investigated and fully identified using FT-IR, SEM, BET/BJH, XRD, EDS, elemental mapping, and TGA/DTG techniques.

After preparing and identifying MIL-88B(Fe_2/Ni)/imidazole/SO_3H as an effective catalyst, this catalyst was used in multi-component reactions and for the preparation of nicotinonitrile derivatives. Examining the reaction conditions showed that the above catalyst had a high ability to produce the desired products in a short period of time (30–40 min.) and high product efficiency (70–85%). FT-IR, ^{1}H-NMR, ^{13}C-NMR and HR-mass analyses were used to further investigate the synthesized products (Scheme 2). Examining the mechanism of the above reaction showed that the stereochemistry of the reaction was on the basis of CVBAO, in which the double bonds act as a bridge between the donor and acceptor orbitals.

Characterization

The physicochemical properties of MIL-88B(Fe_2/Ni)/imidazole/SO_3H as a new acidic catalyst were investigated by different techniques. First, in order to confirm the linking of the functional groups in the structure of the catalyst, the FT-IR technique was used. The FT-IR spectra of MIL-88B(Fe_2/Ni), MIL-88B(Fe_2/Ni)/imidazole, and MIL-88B(Fe_2/Ni)/imidazole/SO_3H clearly showed the different stages of the catalyst synthesis, as can be seen in Fig. 3. The broad peak in the region of 2500–3500 cm^{-1} was related to the OH stretching vibration of the acidic group SO_3H. Also, the absorption bands in the 1100 and 1141 cm^{-1} regions represent the stretching vibrations of N–S and O–S. The absorption band observed at 1689 cm^{-1} was attributed to carbonyl groups (C=O). Comparison of the patterns for the different stages of catalyst synthesis well showed the increase in imidazole, and SO_3H groups in MIL-88B(Fe_2/Ni), which indicated the successful synthesis of the presented catalyst.

Next, scanning electron microscopy (SEM) analysis was used to study the morphology of the formed structures. Consequently, the morphology of MIL-88B(Fe_2/Ni), MIL-88B(Fe_2/Ni)/imidazole, and MIL-88B(Fe_2/Ni)/imidazole/SO_3H were compared (Fig. 4). As can be seen from the SEM images, MIL-88B(Fe_2/Ni) displayed

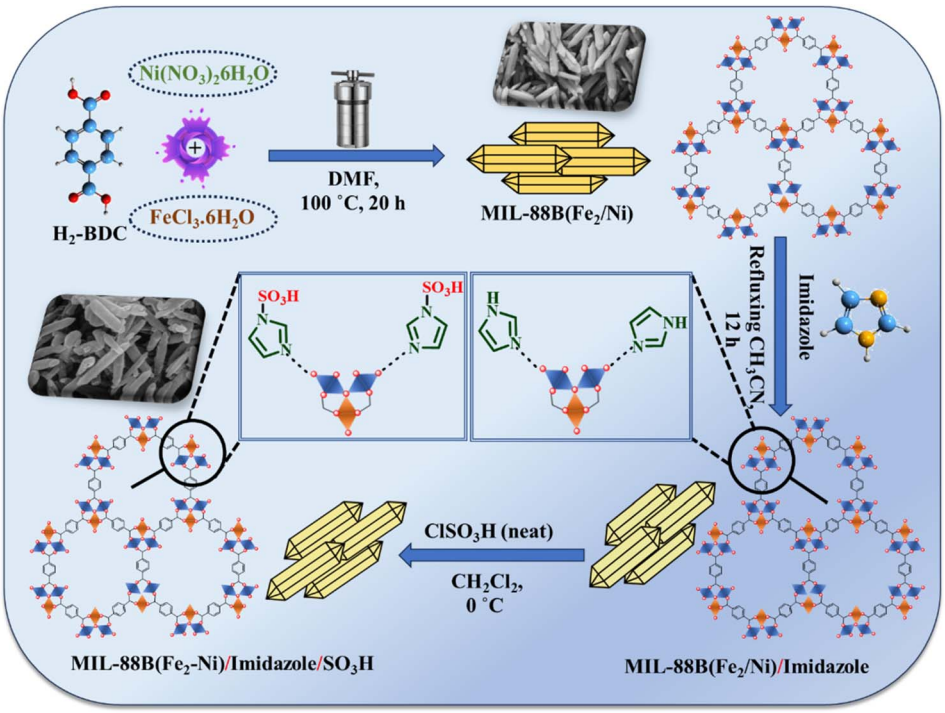

Scheme 1 Schematic general strategy for the preparation of MIL-88B(Fe_2/Ni)/imidazole/SO_3H as a new porous catalyst.

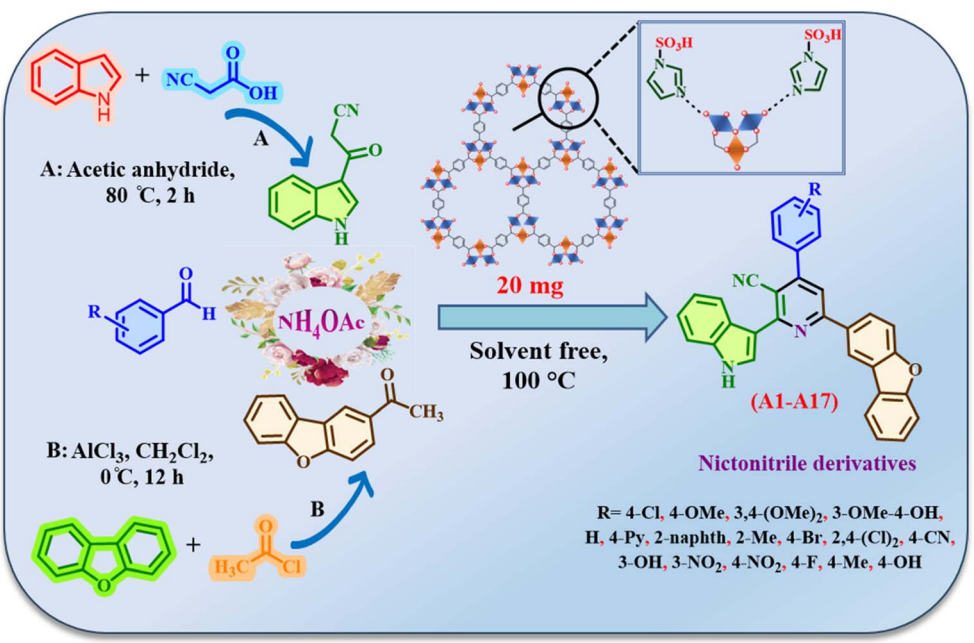

Scheme 2 Preparation of new nicotinonitrile derivatives using MIL-88B(Fe_2/Ni)/imidazole/SO_3H.

the morphology of a uniform rod-shaped crystal (Fig. 4a). It should be noted that the size of each rod-shaped crystal was about 1 μm and had an average diameter of 110 nm. This large size of nanorods caused various functional groups to be placed well on the surface of each of the rod-shaped crystals. Therefore, the increase in imidazole (Fig. 4b) and chlorosulfonic acid (Fig. 4c) was achieved on the surface of the primary structure without showing a significant change in the morphology of the primary nanorods. As can be seen from the SEM images, the proper morphology and the preservation of the morphology

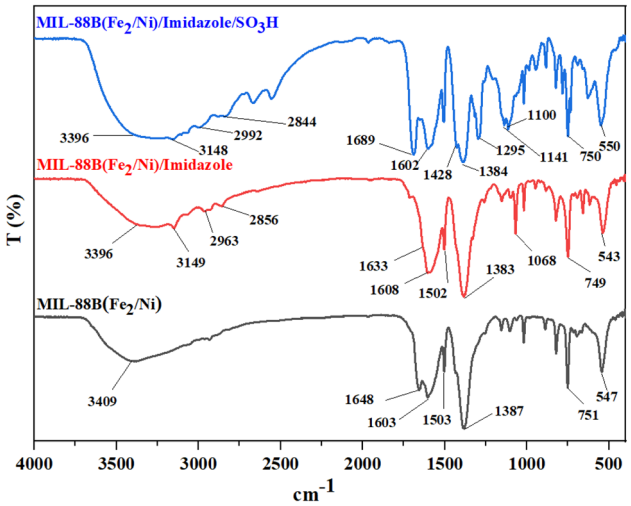

Fig. 3 FT-IR spectra for the different stages of synthesis of MIL-88B(Fe_2/Ni)/imidazole/SO_3H.

indicate MIL-88B(Fe_2/Ni)/imidazole/SO_3H would be as an efficient catalyst for carrying out organic reactions.

In order to investigate the growth of the crystal plates, the X-ray powder diffraction (XRD) technique was used. The XRD pattern of MIL-88B(Fe_2/Ni) was found to be in good agreement with previous reports.[46] For further investigation, the XRD patterns of MIL-88B(Fe_2/Ni), MIL-88B(Fe_2/Ni)/imidazole, and MIL-88B(Fe_2/Ni)/imidazole/SO_3H were obtained and are compared in Fig. 5. The results show that the crystal pattern was preserved after two steps of increase and the small changes observed were due to the increase in imidazole and chlorosulfonic acid groups. The stability of the crystal structure may be the major reason for the good performance of this catalyst in the production of desired products.

Next, energy-dispersive X-ray spectroscopy (EDS) and elemental mapping techniques were used to check out the presence of the elements in the catalyst structure. Fig. 6a shows the presence of iron (Fe), nickel (Ni), oxygen (O) and carbon (C) elements. Comparing Fig. 6a and b, it could be seen that there was an increase in sulfur (S) and nitrogen (N) elements (Fig. 6b) in the final catalyst. The uniform distribution of the elements was also examined, as shown in Fig. 6c, in which it could be seen that the elements carbon (orange), nickel (green), oxygen (purple), sulfur (blue), iron (red), and nitrogen (phosphorus) were uniformly distributed. It should be noted that the results obtained from the EDS and elemental mapping were in good agreement with each other and thus confirmed the structure of the desired catalyst.

Thermogravimetric (TGA) and differential thermogravimetric (DTG) analyses were used to check the thermal and

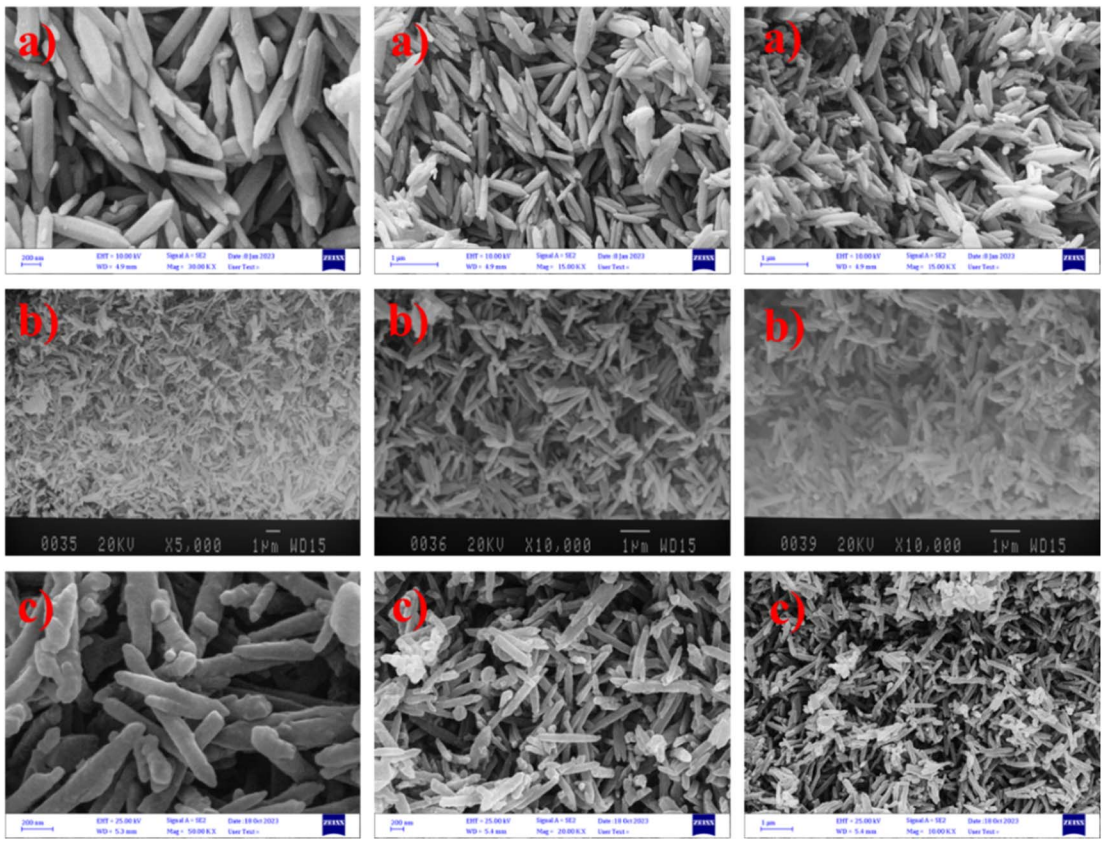

Fig. 4 Scanning electron microscopy (SEM) images of (a) MIL-88B(Fe_2/Ni), (b) MIL-88B(Fe_2/Ni)/imidazole, and (c) MIL-88B(Fe_2/Ni)/imidazole/SO_3H.

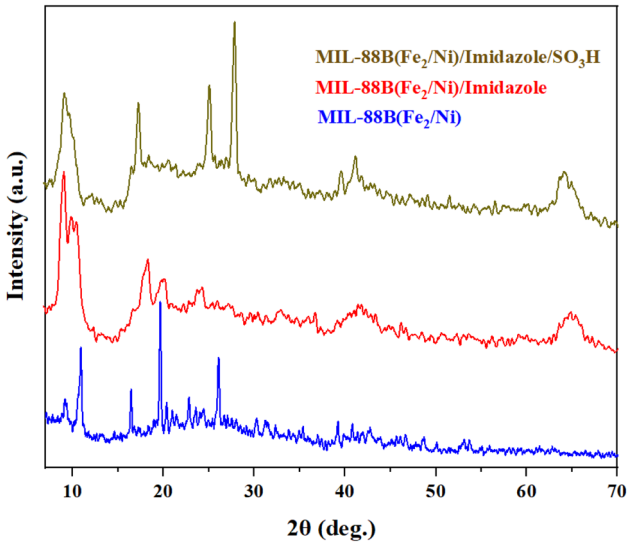

Fig. 5 Comparison of the XRD patterns at different stages of the synthesis of MIL-88B(Fe_2/Ni)/imidazole/SO_3H.

chemical stability of the MIL-88B(Fe_2/Ni)/imidazole/SO_3H. According to the results obtained in Fig. 7, four separate stages of decomposition could be observed. The first loss in the temperature range of 100–120 °C was caused by the removal of the solvent that remained in the catalyst structure during the synthesis and purification. The next loss occurred in the temperature range up to 270 °C, which was probably related to the destruction of the acidic bond (SO_3H) and the removal of this group from the surface of the catalyst. The next losses occurred at 450 °C and 550 °C and were related to the decomposition of the MOF. According to the results obtained from the above analysis, the desired catalyst can act as a catalyst for proceeding organic reactions up to a temperature of 270 °C. It is worth mentioning that the synthesis of nicotinonitrile derivatives is carried out at a temperature of 100 °C, so MIL-88B(Fe_2/Ni)/imidazole/SO_3H would be an effective catalyst for the synthesis of the mentioned compounds.

In another study to evaluate the textural properties of MIL-88B(Fe_2/Ni)/imidazole/SO_3H, N_2 adsorption and desorption isotherms were used. The surface area calculated based on the Brunauer–Emmett–Teller (BET) equation and the total pore volume were 49.95 $m^2\ g^{-1}$ and 0.166 $cm^3\ g^{-1}$, respectively (Fig. 8a). Next, the BJH method was used to check the pore size distribution of the structures. According to the obtained results, the mean pore diameter was 13.31 nm (Fig. 8b).

After analyzing the topographical structure of MIL-88B(Fe_2/Ni)/imidazole/SO_3H, it was used as a bimetallic-MOF catalyst containing acidic groups in the preparation of nicotinonitrile derivatives. For this purpose, the reaction between 3-(1*H*-indol-3-yl)-3-oxopropanenitrile (1 mmol, 0.184 g), 1-(dibenzo[*b*,*d*]furan-2-yl)ethan-1-one (1 mmol, 0.21 g), 4-chlorobenzaldehyde (1 mmol, 0.14 g), and ammonium acetate (1.5 mmol, 0.11 g) was chosen as the model reaction. The optimal conditions, including the choice of solvent type, required temperature, and amounts of catalyst, are shown in Table 1. The model reaction was carried out in different organic solvents and in solvent-free conditions, and according to the results the reaction under solvent-free conditions had the highest efficiency. Examining the changes in

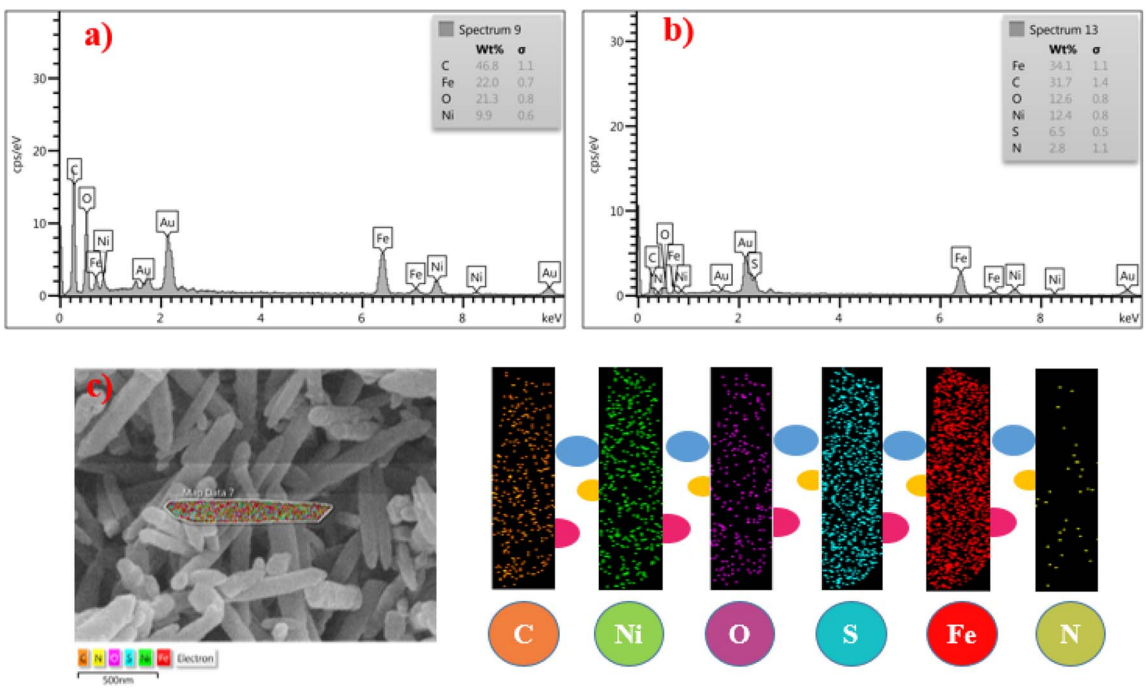

Fig. 6 Energy-dispersive X-ray spectroscopy (EDS): (a and b) MIL-88B(Fe_2/Ni) (a) and MIL-88B(Fe_2/Ni)/imidazole/SO_3H (b). Elemental mapping of MIL-88B(Fe_2/Ni)/imidazole/SO_3H (c).

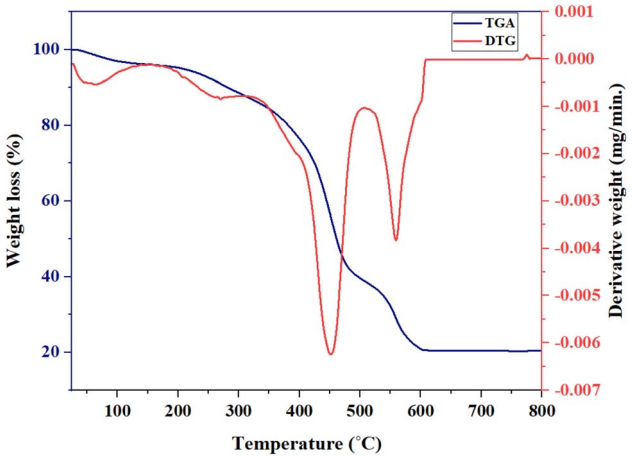

Fig. 7 Thermogravimetric (TGA) and differential thermogravimetric (DTG) analyses of MIL-88B(Fe_2/Ni)/imidazole/SO_3H.

temperature and the use of different amounts of catalyst showed that a temperature of 100 °C and a catalyst amount of 20 mg were the best conditions for the above reaction.

After choosing the optimal reaction conditions, a wide range of nicotinonitriles were synthesized under green and mild conditions by using different aromatic aldehydes (including with electron-donating and electron-withdrawing functional groups). According to the results listed in Table 2, MIL-88B(Fe_2/Ni)/imidazole/SO_3H demonstrated a suitable efficiency (70–85%) and a short time (30–40 min) to perform the reaction in the synthesis of the desired compounds.

It is believed that the presence of uniform rod-shaped morphologies with large dimensions caused the SO_3H groups to be placed well on the surface of the catalyst, making it a suitable substrate for organic reactions. Therefore, in the proposed mechanism, first the carbonyl functional group of 1-(dibenzo[*b*,*d*]furan-2-yl)ethan-1-one is activated by the catalyst and reacts with *in situ* generated ammonia arising from the thermal dissociation of ammonium acetate to obtain

Table 1 Optimization of some reaction parameters using MIL-88B(Fe_2/Ni)/imidazole/SO_3H as a new porous catalyst

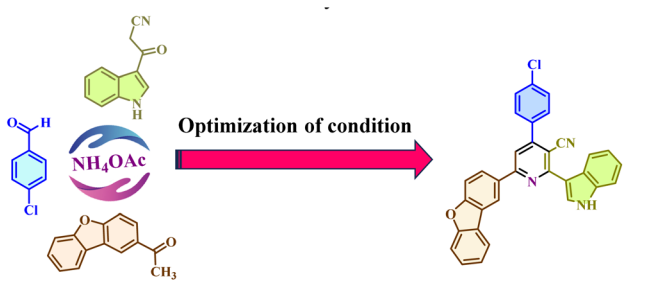

Entry	Solvent	Catalyst (mg)	Temp. (°C)	Time (h)	Yield (%)
1	—	25	100	0.75	70
2	—	20	100	0.5	85
3	—	15	100	0.67	75
4	—	10	100	0.84	60
5	—	5	100	1	50
6	MeOH	20	Reflux	8	45
7	EtOH	20	Reflux	9	40
8	CH_3CN	20	Reflux	12	—
9	EtOAc	20	Reflux	10	20
10	CH_2Cl_2	20	Reflux	12	—
11	DMF	20	Reflux	10	40
12	$CHCl_3$	20	Reflux	14	20
13	—	20	110	0.58	80
14	—	20	80	0.67	70
15	—	20	50	0.92	40
16	—	20	25	1.5	—

intermediate **I** *via* tautomerization. In another part of the reaction, the carbonyl functional group of the aldehydes is activated by the catalyst and performs the condensation of Knoevenagel with 3-(1*H*-indol-3-yl)-3-oxopropanenitrile and intermediate **II** is then obtained. Next, intermediate **I** reacts with intermediate **II** and intermediate **III** is obtained *via* the tautomerization process. Then, with the attack of the amine

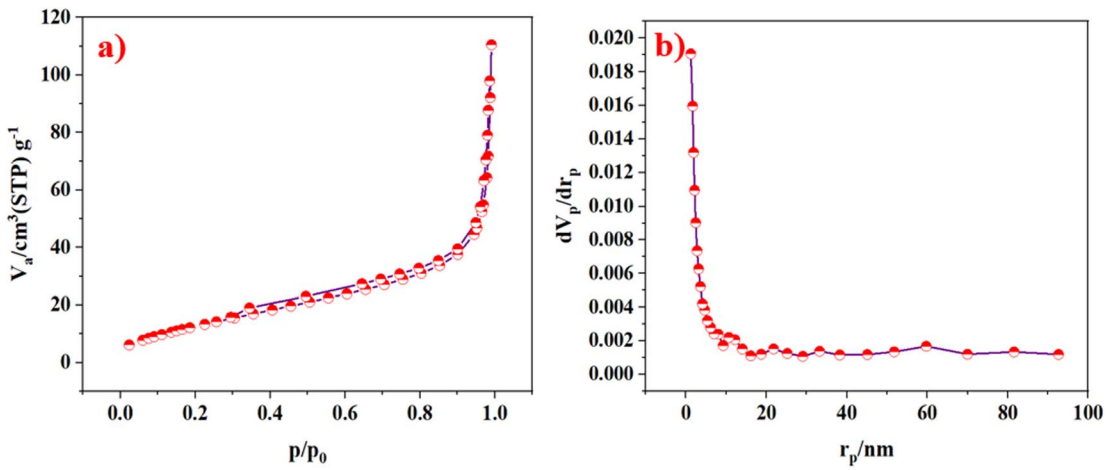

Fig. 8 (a) N_2 adsorption–desorption isotherms and (b) pore size distribution of MIL-88B(Fe_2/Ni)/imidazole/SO_3H.

Table 2 Molecular structures of the desired synthesized nicotinonitrile derivatives obtained using MIL-88B(Fe_2/Ni)/imidazole/SO_3H as a new porous catalyst

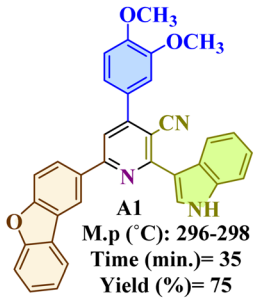

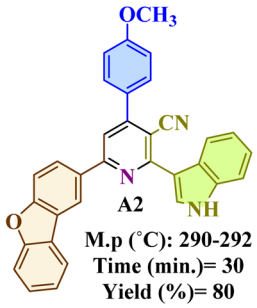

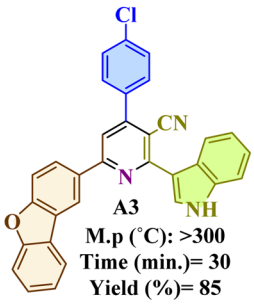

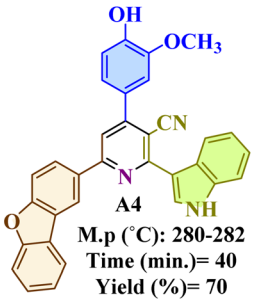

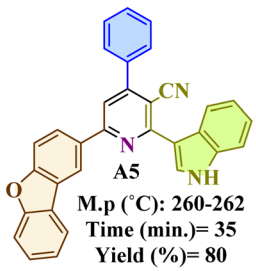

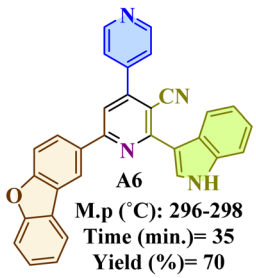

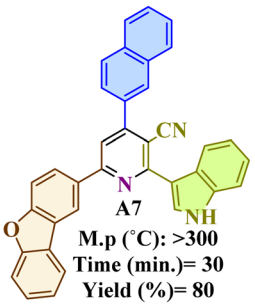

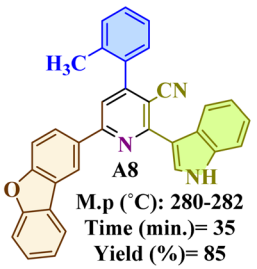

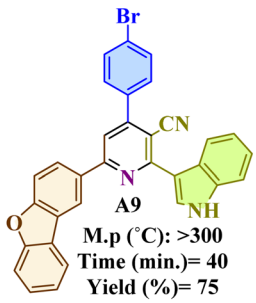

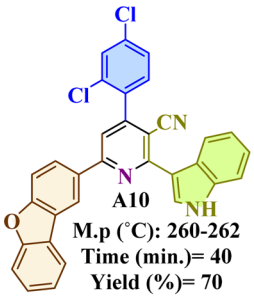

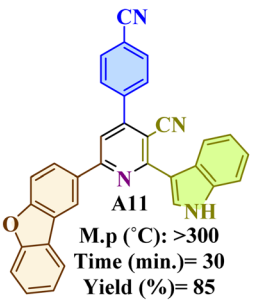

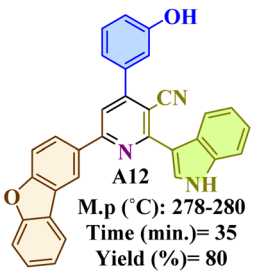

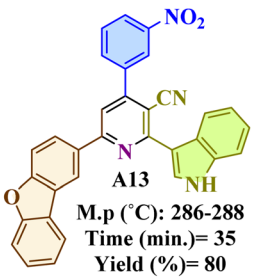

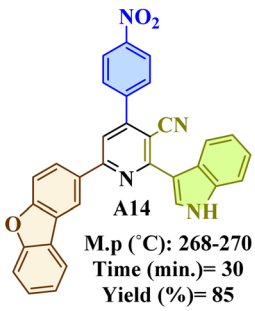

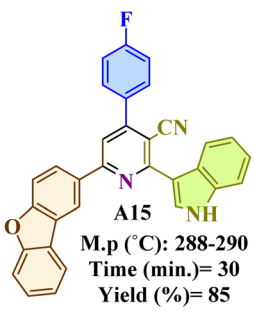

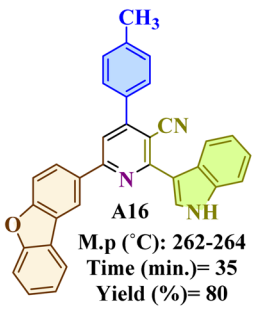

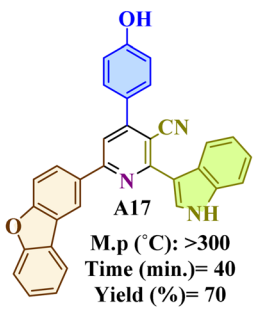

Table 3 Comparison of the performance of various catalysts in the synthesis of new nicotinonitrile derivatives

Entry	Catalyst	Amount of cat. (mol%)	Time (min)	Yield (%)
1	MIL-88B(Fe_2/Ni)/imidazole/SO_3H	20 mg	30	85
2	MIL-88B(Fe_2/Ni)[46]	20 mg	70	45
3	Co-MOF-71/imidazole/SO_3H[24]	20 mg	60	65
4	Co(BDC-NH$(CH_2)_4SO_3H$)[22]	20 mg	70	40
5	Et_3N	20	120	35
6	NaOH	20 mg	150	20
7	H_2SO_4	20	90	35
8	Pipyridine	20	130	20
9	CQDs-N$(CH_2PO_3H_2)_2$/SBA-15 (ref. 47)	20 mg	60	50
10	CQDs-N$(CH_2PO_3H_2)_2$ (ref. 48)	20 mg	50	55
11	Ti-MOF-UR[49]	20 mg	70	50
12	MIL-88B(Fe_2/Co)-UR[50]	20 mg	50	60
13	SSA[42]	20 mg	100	20
14	*p*-TSA	20 mg	70	35

group on the carbonyl group, intramolecular cyclization occurs and intermediate **IV** is formed. This intermediate creates intermediate **V** by removing a water (H_2O) molecule. Finally, intermediate **V** is converted to the corresponding pyridine derivatives *via* a cooperative vinylogous anomeric-based oxidation (CVABO) mechanism, and this can be through the exit of the H_2 or H_2O_2 molecule (Scheme 3).[24,25]

In order to further investigate the catalytic capability of MIL-88B(Fe_2/Ni)/imidazole/SO_3H, the model reaction of 3-(1*H*-indol-3-yl)-3-oxopropanenitrile (1 mmol, 0.184 g), 1-(dibenzo[*b*,*d*]furan-2-yl)ethan-1-one (1 mmol, 0.21 g), 4-chlorobenzaldehyde (1 mmol, 0.14 g), and ammonium acetate (1.5 mmol, 0.11 g) was carried out using different organic and inorganic catalysts as well as the previous precursors and stages of the catalyst. The results obtained are listed in Table 3 and show that none of the used catalysts had a better performance than MIL-88B(Fe_2/Ni)/imidazole/SO_3H for the preparation of nicotinonitriles. This suggests the above catalyst could be used in the preparation of other organic compounds and probably the target products will be obtained with a suitable efficiency. Next, the recyclability of the catalyst was investigated. The results are shown in Fig. 9. MIL-88B(Fe_2/Ni)/imidazole/SO_3H as an acidic porous catalyst could be used up to four times without a significant change in the efficiency and reaction time.

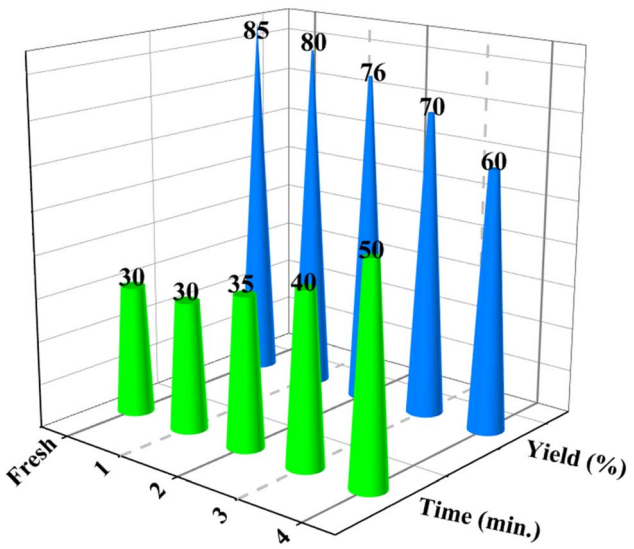

Fig. 9 Recyclability of MIL-88B(Fe_2/Ni)/imidazole/SO_3H in the synthesis of nicotinonitrile derivatives.

According to the mentioned items, the compounds nicotinitriles, indole, pyridine, and dibenzofuran have many biological properties, such as anti-cancer, antibacterial, and antifungal.[26,27] Therefore, according to the structure of the synthesized products, we investigated the antibacterial properties of these compounds and catalysts. Specifically, their antibacterial activities against *E. coli* (Gram-negative bacteria), *S. aureus* (Gram-positive bacteria), and MRSA were investigated under laboratory conditions using the CFU method. The results are depicted in Fig. 10.

The antimicrobial sensitivity test results showed that compound A1 inhibited *S. aureus* and *E. coli* by 100%, making it a favorable antibacterial for these bacteria. However, its inhibition rate against MRSA was 83%. On the other hand, MIL-88B(Fe_2/Ni)/imidazole/SO_3H exhibited inhibition rates of 10.32% for *E. coli*, 89% for *S. aureus*, and 74% for MRSA. These results indicate that MIL-88B(Fe_2/Ni)/imidazole/SO_3H was more effective against Gram-positive bacteria compared to Gram-negative ones.

Fig. 10 demonstrates the varying antimicrobial effects of the synthesized compounds on both Gram-positive and Gram-negative bacterial species. Additionally, the synthesized compounds were tested using the disk diffusion susceptibility method, although the specific data are not presented. However, they exhibited no antibacterial activity in this test. It is important to note that their lack of antibacterial activity in these tests was attributed to their insolubility in normal saline.

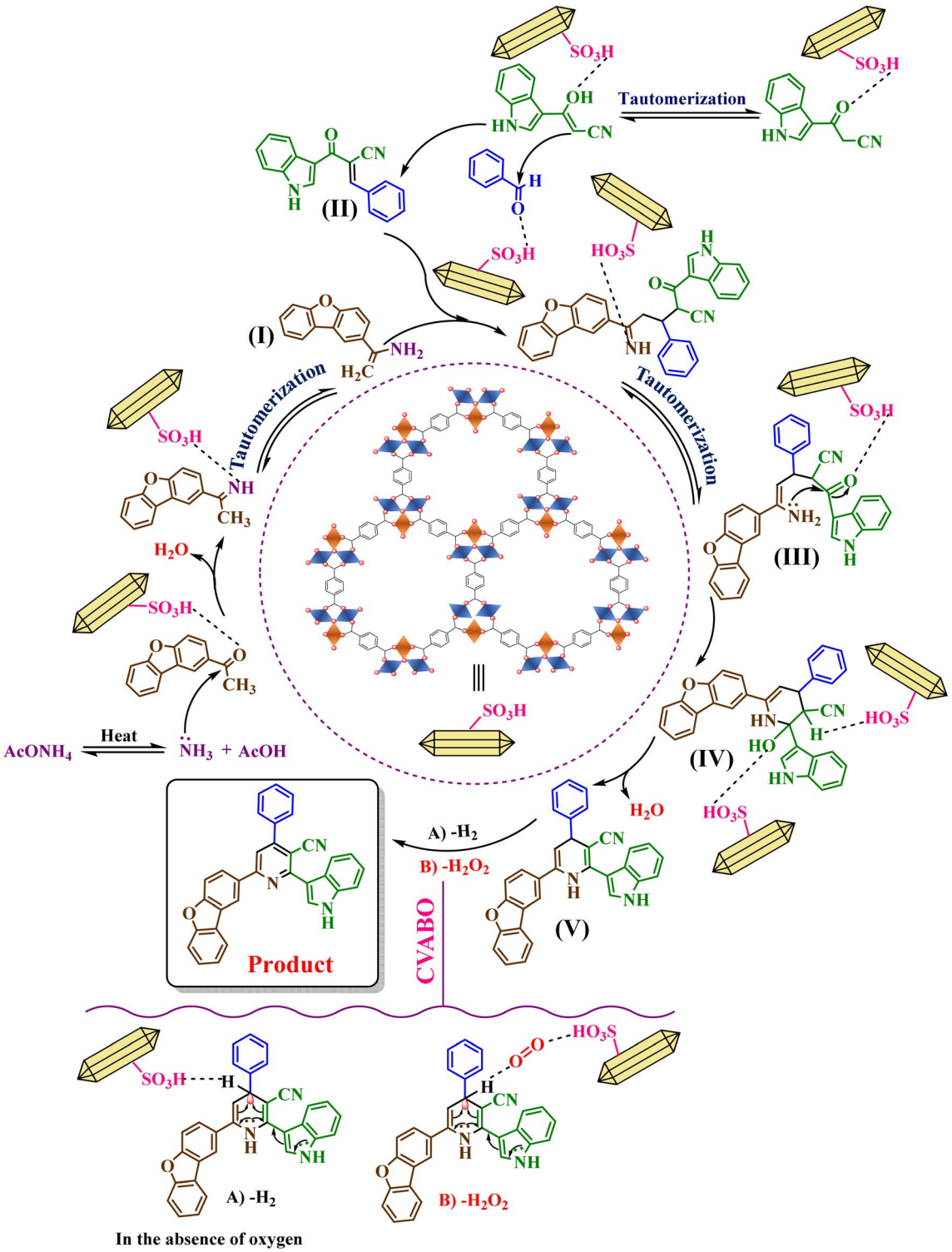

Scheme 3 Proposed mechanism for the synthesis of nicotinitriles using MIL-88B(Fe_2/Ni)/imidazole/SO_3H as a new porous catalyst.

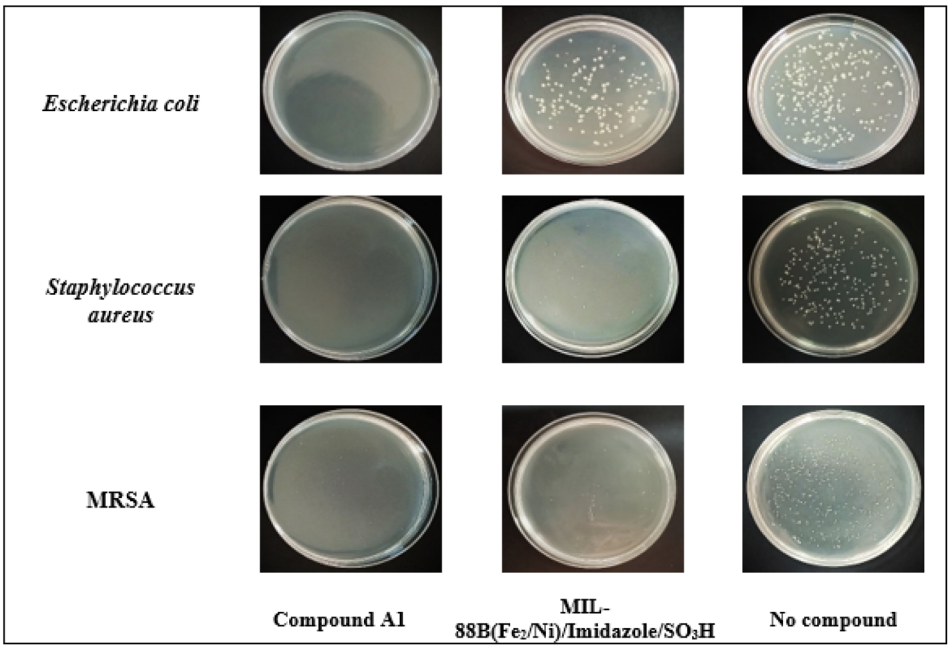

Fig. 10 Examining the antibacterial activity of compound A1 and MIL-88B(Fe_2/Ni)/imidazole/SO_3H against *Staphylococcus aureus*, *Escherichia coli*, and MRSA bacteria.

Conclusion

In summary, the aim of this research was the development of bimetallic-MOFs as an emerging generation of heterogeneous porous catalysts. MIL-88B(Fe_2/Ni), which contains iron (Fe) and nickel (Ni) metals, was designed and synthesized. Then, with the help of a post-modification strategy, MIL-88B(Fe_2/Ni)/imidazole/SO_3H was synthesized as a porous acid catalyst. The structure and physicochemical properties of the above catalyst were well determined using FT-IR, SEM, BET/BJH, XRD, EDS, elemental mapping, and TGA/DTG techniques. This catalyst was used to prepare nicotinonitrile derivatives with indole and dibenzofuran biological scaffolds. The main advantages of the described method include the good yield of products, short reaction time, synthesis under mild and green conditions, and the ability to recycle the catalyst. In addition, MIL-88B(Fe_2/Ni)/imidazole/SO_3H and compound A1 were investigated as antibacterial agents and the results showed that the synthesized product and catalyst had good antibacterial activities.

Data availability

ESI† and spectral data for nicotinonitrile derivatives are freely available and will be provided upon reasonable request from the corresponding author.

Conflicts of interest

The authors declare that they have no known competing financial interests or personal relationships that could have appeared to influence the work reported in this paper.

Acknowledgements

We would like to thank Bu-Ali Sina University and Iran National Science Foundation (INSF) (Grant Number. 4029146) for their financial support.

References

1 R. Shah, S. Ali, F. Raziq, S. Ali, P. M. Ismail, S. Shah, R. Iqbal, X. Wu, W. He, X. Zu, A. Zada, A. Null, F. Mabood, A. Vinu, S. H. Jhung, J. Yi and L. Qiao, Exploration of metal organic frameworks and covalent organic frameworks for energy-related applications, *Coord. Chem. Rev.*, 2023, **477**, 214968.
2 B. Jie, H. Lin, Y. Zhai, J. Ye, D. Zhang, Y. Xie, X. Zhang and Y. Yang, Mechanism, design and application of fluorescent recognition based on metal organic frameworks in pollutant detection, *Chem. Eng. J.*, 2023, **454**, 139931.
3 G. Lin, B. Zeng, J. Li, Z. Wang, S. Wang, T. Hu and L. Zhang, A systematic review of metal organic frameworks materials for heavy metal removal: Synthesis, applications and mechanism, *Chem. Eng. J.*, 2023, **460**, 141710.
4 L. Jiao and H. L. Jiang, Metal–organic frameworks for catalysis: Fundamentals and future prospects, *Chin. J. Catal.*, 2023, **45**, 1–5.
5 F. Yang, M. Du, K. Yin, Z. Qiu, J. Zhao, C. Liu, G. Zhang, Y. Gao and H. Pang, Applications of metal–organic frameworks in water treatment: a review, *Small*, 2022, **18**, 2105715.
6 U. Ryu, S. Jee, P. C. Rao, J. Shin, C. Ko, M. Yoon, K. S. Park and K. M. Choi, Recent advances in process engineering and upcoming applications of metal–organic frameworks, *Coord. Chem. Rev.*, 2021, **426**, 213544.

7 S. Lu, L. Liu, H. Demissie, G. An and D. Wang, Design and application of metal-organic frameworks and derivatives as heterogeneous Fenton-like catalysts for organic wastewater treatment: A review, *Environ. Int.*, 2021, **146**, 106273.
8 L. Chen, H. F. Wang, C. Li and Q. Xu, Bimetallic metal–organic frameworks and their derivatives, *Chem. Sci.*, 2020, **11**, 5369–5403.
9 X. He, D. R. Chen and W. N. Wang, Bimetallic metal-organic frameworks (MOFs) synthesized using the spray method for tunable CO_2 adsorption, *Chem. Eng. J.*, 2020, **382**, 122825.
10 Z. Zhu, Y. Zeng, Z. Pei, D. Luan, X. Wang and X. W. Lou, Bimetal-Organic Framework Nanoboxes Enable Accelerated Redox Kinetics and Polysulfide Trapping for Lithium–Sulfur Batteries, *Angew Chem. Int. Ed. Engl.*, 2023, **62**, e202305828.
11 A. Kumari, S. Kaushal and P. P. Singh, Bimetallic metal organic frameworks heterogeneous catalysts: design, construction, and applications, *Mater. Today Energy*, 2021, **20**, 100667.
12 M. Li, J. Yuan, G. Wang, L. Yang, J. Shao, H. Li and J. Lu, One-step construction of Ti-In bimetallic MOFs to improve synergistic effect of adsorption and photocatalytic degradation of bisphenol A, *Sep. Purif. Technol.*, 2022, **298**, 121658.
13 B. Iqbal, M. Saleem, S. N. Arshad, J. Rashid, N. Hussain and M. Zaheer, One-pot synthesis of heterobimetallic metal–organic frameworks (MOFs) for multifunctional catalysis, *Chem. Eur. J.*, 2019, **25**, 10490–10498.
14 J. Wang, J. Wang, M. Zhang, S. Li, R. Liu and Z. Li, Metal-organic frameworks-derived hollow-structured iron-cobalt bimetallic phosphide electrocatalysts for efficient oxygen evolution reaction, *J. Alloys Compd.*, 2020, **821**, 153463.
15 M. M. Rasooll, H. Sepehrmansourie, M. Zarei, M. A. Zolfigol, M. Hosseinifard and Y. Gu, Catalytic Application of Functionalized Bimetallic-Organic Frameworks with Phosphorous Acid Tags in the Synthesis of Pyrazolo[4,3-*e*]pyridines, *ACS omega*, 2023, **8**, 25303–25315.
16 D. Sun, F. Sun, X. Deng and Z. Li, Mixed-metal strategy on metal-organic frameworks (MOFs) for functionalities expansion: Co substitution induces aerobic oxidation of cyclohexene over inactive Ni-MOF-74, *Inorg. Chem.*, 2015, **54**, 8639–8643.
17 G. S. More, A. K. Kar and R. Srivastava, Cu-Ce bimetallic metal-organic framework-derived, oxygen vacancy-boosted visible light-active Cu_2O–CeO_2/C heterojunction: An efficient photocatalyst for the Sonogashira coupling reaction, *Inorg. Chem.*, 2022, **61**, 19010–19021.
18 A. Tiwari, P. S. Sagara, V. Varma and J. K. Randhawa, Bimetallic Metal Organic Frameworks as Magnetically Separable Heterogeneous Catalyst for Efficient Organic Transformation and Photocatalytic Dye Degradation, *ChemPlusChem*, 2019, **84**, 136.
19 Y. Hu, J. Zhang, H. Huo, Z. Wang, X. Xu, Y. Yang, K. Lin and R. Fan, One-pot synthesis of bimetallic metal-organic frameworks (MOFs) as acid-base bifunctional catalysts for tandem reaction, *Catal. Sci. Technol.*, 2020, **10**, 315–322.
20 E. Tavakoli, H. Sepehrmansourie, M. A. Zolfigol, A. Khazaei, A. Mohammadzadeh, E. Ghytasranjbar and M. A. As' Habi, Synthesis and Application of Task-Specific Bimetal–Organic Frameworks in the Synthesis of Biological Active Spiro-Oxindoles, *Inorg. Chem.*, 2024, **63**, 5805–5820.
21 E. Tavakoli, H. Sepehrmansourie, M. Zarei, M. A. Zolfigol, A. Khazaei and M. A. As' Habi, Application of Zr-MOFs based copper complex in synthesis of pyrazolo[3,4-*b*]pyridine-5-carbonitriles *via* anomeric-based oxidation, *Sci. Rep.*, 2023, **13**, 9388.
22 F. Jalili, H. Sepehrmansourie, M. Zarei, M. A. Zolfigol, A. Khazaei and M. A. As' Habi, Application of novel metal-organic frameworks containing sulfonic acid pendings in synthesis of chromeno[4,3-*d*]pyrimidines *via* back to back anomeric based oxidation, *Arabian J. Chem.*, 2024, **17**, 105635.
23 S. Kalhor, H. Sepehrmansourie, M. Zarei, M. A. Zolfigol and H. Shi, Application of Functionalized Zn-Based Metal–Organic Frameworks (Zn-MOFs) with CuO in Heterocycle Synthesis *via* Azide-Alkyne Cycloaddition, *Inorg. Chem.*, 2024, **63**, 4898–4914.
24 H. Sepehrmansourie, M. Mohammadi Rasooll, M. Zarei, M. A. Zolfigol and Y. Gu, Application of metal-organic frameworks with sulfonic acid tags in the synthesis of pyrazolo[3,4-*b*]pyridines *via* a cooperative vinylogous anomeric-based oxidation, *Inorg. Chem.*, 2023, **62**, 9217–9229.
25 H. Ahmadi, M. Zarei and M. A. Zolfigol, Catalytic Application of a Novel Basic Alkane–sulfonate Metal–organic Frameworks in the Preparation of Pyrido[2,3-*d*]pyrimidines *via* a Cooperative Vinylogous Anomeric-based Oxidation, *ChemistrySelect*, 2022, **7**, e202202155.
26 E. R. Kotb, M. A. El-Hashash, M. A. Salama, H. S. Kalf and N. A. Abdel Wahed, Synthesis and reactions of some novel nicotinonitrile derivatives for anticancer and antimicrobial evaluation, *Acta Chim. Slov.*, 2009, **56**, 908–919.
27 M. A. Gouda, E. Attia, M. H. Helal and M. A. Salem, Recent Progress on Nicotinonitrile Scaffold-based Anticancer, Antitumor, and Antimicrobial Agents: A Literature Review, *J. Heterocycl. Chem.*, 2018, **55**, 2224–2250.
28 K. Kaur and V. Jaitak, Recent development in indole derivatives as anticancer agents for breast cancer, *Anti-Cancer Agents Med. Chem.*, 2019, **19**, 962–983.
29 A. A. Bekhit, A. Hymete, A. Damtew, A. M. I. Mohamed and A. E. D. A. Bekhit, Synthesis and biological screening of some pyridine derivatives as anti-malarial agents, *J. Enzyme Inhib. Med. Chem.*, 2012, **27**, 69–77.
30 G. O. M. Moustafa, A. S. Al-Wasidi, A. M. Naglah and M. Refat, Synthesis of dibenzofuran derivatives possessing anticancer activities: A review, *Egypt. J. Chem.*, 2020, **63**, 2355–2367.
31 I. V. Alabugin, L. Kuhn, M. G. Medvedev, N. V. Krivoshchapov, V. A. Vil, I. A. Yaremenko, P. Mehaffy, M. Yarie, A. O. Terent'ev and M. A. Zolfigol, Stereoelectronic power of oxygen in control of chemical

reactivity: the anomeric effect is not alone, *Chem. Soc. Rev.*, 2021, **50**, 10253–10345.

32 I. V. Alabugin, L. Kuhn, N. V. Krivoshchapov, P. Mehaffy and M. G. Medvedev, Anomeric effect, hyperconjugation and electrostatics: Lessons from complexity in a classic stereoelectronic phenomenon, *Chem. Soc. Rev.*, 2021, **50**, 10212–10252.

33 M. Yarie, Catalytic anomeric based oxidation, *Iran. J. Catal.*, 2017, **7**, 85–88.

34 M. Yarie, Spotlight: Catalytic vinylogous anomeric based oxidation (Part I), *Iran. J. Catal.*, 2020, **10**, 79–83.

35 B. Danishyar, H. Sepehrmansourie, H. Ahmadi, M. Zarei, M. A. Zolfigol and M. Hosseinifard, Application of Nanomagnetic Metal–Organic Frameworks in the Green Synthesis of Nicotinonitriles *via* Cooperative Vinylogous Anomeric-Based Oxidation, *ACS omega*, 2023, **8**, 18479–18490.

36 M. R. Anizadeh, M. A. Zolfigol, M. Torabi, M. Yarie and B. Notash, Urea-dithiocarbamic acid functionalized magnetic nanoparticles modified with Ch-Cl: Catalytic application for the synthesis of novel hybrid pyridones *via* cooperative geminal-vinylogous anomeric-based oxidation, *J. Mol. Liq.*, 2022, **364**, 120016.

37 (*a*) C. B. Bai, N. X. Wang, Y. Xing and X. W. Lan, Progress on chiral NAD (P) H model compounds, *Synlett*, 2017, **28**, 402–414; (*b*) G. Hamasaka, H. Tsuji and Y. Uozumi, Organoborane-catalyzed hydrogenation of unactivated aldehydes with a Hantzsch ester as a synthetic NAD (P) H analogue, *Synlett*, 2015, **26**, 2037–2041.

38 M. A. Zolfigol, S. Azizian, M. Torabi, M. Yarie and B. Notash, The importance of non-stoichiometric ratio of reactants in organic synthesis, *J. Chem. Educ.*, 2024, **101**, 877–881.

39 X. Zhao, P. Pachfule, S. Li, J. R. J. Simke, J. Schmidt and A. Thomas, Bifunctional electrocatalysts for overall water splitting from an iron/nickel-based bimetallic metal-organic framework/dicyandiamide composite, *Angew. Chem.*, 2018, **130**, 9059–9064.

40 R. M. Abdel-Motaleb, A. M. A. S. Makhloof, H. M. Ibrahim and M. H. Elnagdi, Studies with azoles and benzoazoles: a novel simple approach for synthesis of 3-functionally substituted 3-acylindoles, *J. Heterocycl. Chem.*, 2007, **44**, 109–114.

41 S. Kantevari, T. Yempala, P. Yogeeswari, D. Sriram and B. Sridhar, Synthesis and antitubercular evaluation of amidoalkyl dibenzofuranols and 1*H*-benzo[2,3]benzofuro [4,5-*e*][1,3]oxazin-3(2*H*)-ones, *Bioorg. Med. Chem. Lett.*, 2011, **21**, 4316–4319.

42 M. A. Zolfigol, Silica sulfuric acid/$NaNO_2$ as a novel heterogenous system for production of thionitrites and disulfides under mild conditions, *Tetrahedron*, 2001, **57**, 9509.

43 P. Salehi, M. A. Zolfigol, F. Shirini and M. Baghbanzadeh, Silica sulfuric acid and silica chloride as efficient reagents for organic reactions, *Curr. Org. Chem.*, 2006, **10**, 2171–2189.

44 H. Sepehrmansourie, H. Alamgholiloo, M. A. Zolfigol, N. N. Pesyan and M. M. Rasooll, Nanoarchitecting a Dual Z-Scheme Zr-MOF/Ti-MOF/g-C_3N_4 Heterojunction for Boosting Gomberg–Buchmann–Hey Reactions under Visible Light Conditions, *ACS Sustain. Chem. Eng.*, 2023, **11**, 3182–3193.

45 H. Sepehrmansourie, H. Alamgholiloo, N. N. Pesyan and M. A. Zolfigol, A MOF-on-MOF strategy to construct double Z-scheme heterojunction for high-performance photocatalytic degradation, *Appl. Catal., B*, 2023, **321**, 122082.

46 G. Huang, F. Zhang, L. Zhang, X. Du, J. Wang and L. Wang, Hierarchical $NiFe_2O_4/Fe_2O_3$ nanotubes derived from metal organic frameworks for superior lithium ion battery anodes, *J. Mater. Chem.*, 2014, **2**, 8048–8053.

47 M. M. Rasooll, H. Sepehrmansourie, M. Zarei, M. A. Zolfigol and S. Rostamnia, Phosphonic acid tagged carbon quantum dots encapsulated in SBA-15 as a novel catalyst for the preparation of N-heterocycles with pyrazolo, barbituric acid and indole moieties, *Sci. Rep.*, 2022, **12**, 20812.

48 M. M. Rasooll, M. Zarei, M. A. Zolfigol, H. Sepehrmansourie, A. Omidi, M. Hasani and Y. Gu, Novel nano-architectured carbon quantum dots (CQDs) with phosphorous acid tags as an efficient catalyst for the synthesis of multisubstituted 4*H*-pyran with indole moieties under mild conditions, *RSC Adv.*, 2021, **11**, 25995–26007.

49 Z. Torkashvand, H. Sepehrmansourie, M. A. Zolfigol and M. A. As' Habi, Application of Ti-MOF-UR as a new porous catalyst for the preparation of pyrazolo[3,4-*b*]quinoline and pyrazolo[4,3-*e*]pyridines, *Mol. Catal.*, 2023, **541**, 113107.

50 M. Mohammadi Rasooll, H. Sepehrmansourie, M. A. Zolfigol, M. Hosseinifard, S. L. Hosseini and Y. Gu, Application of a new porous bimetallic H-bond catalyst in the preparation of biological henna-based pyrazolo[3,4-*b*] quinolines *via* a cooperative vinylogous anomeric based oxidation, *Mol. Catal.*, 2024, **570**, 114628.